Last Millennium Climate and Its Variability in CCSM4

LAURA LANDRUM AND BETTE L. OTTO-BLIESNER

National Center for Atmospheric Research, Boulder, Colorado*

EUGENE R. WAHL

Paleoclimatology Branch, National Climatic Data Center, Boulder, Colorado

ANDREW CONLEY, PETER J. LAWRENCE, NAN ROSENBLOOM, AND HAIYAN TENG

National Center for Atmospheric Research, Boulder, Colorado*

(Manuscript received 15 June 2011, in final form 28 August 2012)

ABSTRACT

An overview of a simulation referred to as the ''Last Millennium'' (LM) simulation of the Community Climate System Model, version 4 (CCSM4), is presented. The CCSM4 LM simulation reproduces many large-scale climate patterns suggested by historical and proxy-data records, with Northern Hemisphere (NH) and Southern Hemisphere (SH) surface temperatures cooling to the early 1800s Common Era by ~0.5°C (NH) and ~0.3°C (SH), followed by warming to the present. High latitudes of both hemispheres show polar amplification of the cooling from the Medieval Climate Anomaly (MCA) to the Little Ice Age (LIA) associated with sea ice increases. The LM simulation does not reproduce La Niña–like cooling in the eastern Pacific Ocean during the MCA relative to the LIA, as has been suggested by proxy reconstructions. Still, dry medieval conditions over the southwestern and central United States are simulated in agreement with proxy indicators for these regions. Strong global cooling is associated with large volcanic eruptions, with indications of multidecadal colder climate in response to larger eruptions. The CCSM4's response to large volcanic eruptions captures some reconstructed patterns of temperature changes over Europe and North America, but not those of precipitation in the Asian monsoon region. The Atlantic multidecadal oscillation (AMO) has higher variance at centennial periods in the LM simulation compared to the 1850 nontransient run, suggesting a long-term Atlantic Ocean response to natural forcings. The North Atlantic Oscillation (NAO), Pacific decadal oscillation (PDO), and El Niño–Southern Oscillation (ENSO) variability modes show little or no change. CCSM4 does not simulate a persistent positive NAO or a prolonged period of negative PDO during the MCA, as suggested by some proxy reconstructions.

1. Introduction

Consistent with our understanding of the records of past forcings, phase 3 of the Paleoclimate Modeling Intercomparison Project (PMIP3) and phase 5 of the Coupled Model Intercomparison Project (CMIP5) proposed that modeling groups perform the ''Last Millennium'' simulation [LM; 850–1850 Common Era (dropped hereafter)] with the same models and at the same resolutions as simulations being done to simulate the twentieth century and into the future. The purpose of such simulations is threefold. First, the simulations would allow an evaluation of the capability of models to capture observed variability on multidecadal and longer time scales. Second, they would—through comparison to long CMIP5 ''unforced'' preindustrial control simulations—provide a means of assessing what portion of the variability is attributable to external forcing and what portion reflects purely internal variability. And third, the simulations would be useful in providing a longer-term perspective for detection and attribution studies.

* The National Center for Atmospheric Research is sponsored by the National Science Foundation.

Corresponding author address: Laura Landrum, NCAR, P.O. Box 3000, Boulder, CO 80307.
E-mail: landrum@ucar.edu

DOI: 10.1175/JCLI-D-11-00326.1

Over the last two decades, numerous reconstructions of Northern Hemisphere (NH) temperature for much or all of the last 1300+ years have been constructed from networks of a variety of proxy data and archives, including tree-ring width and density, boreholes, ice cores, speleothems, charcoal records, lake sediments, documentary evidence, and coral growth. These reconstructions in general confirm to the so-called hockey stick behavior of surface temperatures: NH average cooling from the early portion of the second millennium—the so-called Medieval Climate Anomaly (MCA)—into the Little Ice Age (LIA), and then warming in the second half of the twentieth century to average temperatures outside the range of the previous 1300 years [see Jansen et al. (2007) for a review]. Differences in geographic coverage of the proxy records, including latitudinal distribution and terrestrial versus marine location, along with variation in seasonal focus likely affect the magnitude of the decadal to centennial variability among the temperature reconstructions (Jones et al. 2009). Additionally, the geographic coverage of available proxy records decreases back in time and is less extensive for the first half of the last millennium and earlier.

Numerical climate models provide a means of separating the changes associated with the external forcings of the last millennium from those reflecting internal variability. Models of varying complexity, from energy balance models (Crowley et al. 2003) to Earth models of intermediate complexity (Goosse et al. 2005) to full atmosphere–ocean general circulation models (AOGCMs; Ammann et al. 2007; Servonnat et al. 2010; Jungclaus et al. 2010) have been used to simulate this period [a complete list of last millennium simulations assessed in the Intergovernmental Panel on Climate Change Fourth Assessment Report (IPCC AR4) can be found in Jansen et al. (2007)]. The simpler models, able to run ensembles of simulations, have allowed more exploration of the uncertainties of the forcings and internal variability. The AOGCMs—with more extensive representations of the processes within and between the climate system components—have permitted more detailed examinations of the spatial and temporal variations during the last millennium in comparison to the proxy data.

The Medieval Climate Anomaly, defined by Mann et al. (2009) to be from 950 to 1250, although with significant variation in timing at both hemispheric (Mann et al. 2009) and regional scales (e.g., Wahl et al. 2011), has received considerable attention because of its important role for detection and attribution studies focused on whether the last 50 years is indeed warmer than the MCA, on average, and why. Medieval global average temperatures have been reconstructed to be cooler than recent levels (Mann et al. 2008; noting that the upper range of the estimated 95% confidence intervals is near recent levels for brief periods). Proxy records available for the MCA indicate important differences in the regional, seasonal, and temporal expressions of warmth (Mann et al. 2009; Bradley et al. 2003). Mann et al. (2009) find that although the medieval warmth exceeds the 1961–90 reference period in some regions, particularly in the North Atlantic Ocean, other regions such as the eastern tropical Pacific Ocean were likely cooler than today. Graham et al. (2011) suggest an important role for sea surface temperature (SST) changes and their spatial patterns in the tropical Pacific and Indian Oceans in explaining the observed medieval dynamic circulation changes. Proxy data for the Arctic region indicate a cooling trend from the MCA to the LIA associated with orbital forcing; this cooling reversed to warming in the twentieth century (Kaufman et al. 2009). Evidence of MCA warmth and LIA cooling in Antarctica is less conclusive (Verleyen et al. 2011).

Numerous proxy reconstructions propose that the modes of variability have multidecadal to centennial variability that cannot be captured by the shorter instrumental record. Teleconnection patterns between these modes and regional temperatures and precipitation in the observations have been combined with proxy records of paleoclimate to reconstruct paleorecords of many modes and modal behavior (cf. Wilson et al. 2010; and references therein), along with direct reconstruction of modal behavior from proxy information within a modal region (e.g., Wilson et al. 2010) and utilization of both teleconnected and direct proxy information to systematically reconstruct entire climate fields that include modal regions of interest (e.g., Mann et al. 2009; who reconstruct the annual global surface temperature field by reconstructing its leading EOF patterns for each year). The assumptions in studies that rely on observed teleconnection patterns or proxy information within the modal regions to reconstruct modal behavior are that the modes themselves, and their teleconnections, are stationary (cf. Wilson et al. 2010). However, the spatial character of remote climate responses to climate modes has been shown to vary over the instrumental period (Cole and Cook 1998; Rajagopalan et al. 2000). The reconstruction of leading EOFs of climate fields is less subject to these assumptions, but relies on a related assumption that the retained EOFs, which are derived from instrumental data, form a sufficient basis set for pattern reconstruction in the past (Mann et al. 1998). This assumption has been tested using AOGCM output (Ammann et al. 2007) by Wahl and Smerdon (2012; cf. supplemental online material, section V), who show that it is reasonable within the model experimental context.

Particular interest has focused on whether these modes may have persisted over centuries in a positive or negative phase, potentially explaining climate anomalies of the MCA versus LIA. Trouet et al. (2009) reconstruct a tendency toward a persistent positive-phase NAO during the MCA, which is consistent with reconstructed European summer temperature anomalies (Büntgen and Tegel 2011) that likely track the trajectory of annual temperature as well (Cook et al. 2004a). MacDonald and Case (2005) find a prolonged period of negative-phase Pacific decadal oscillation (PDO) during the MCA that is contemporaneous with a severe megadrought in the western United States. A combination of data reconstruction and modeling work suggests that modal behavior can be forced from one phase of a mode to another for several years to as long as a century by explosive volcanic eruptions and long-term variations in solar irradiance. Reconstructions indicate an increased probability of El Niño events in the two years following tropical volcanic eruptions followed by a rebound to La Niña–type conditions (Adams et al. 2003; cf. D'Arrigo et al. 2009), with modeling studies suggesting a complex interplay of positive and negative feedbacks (e.g., McGregor and Timmermann 2011). Reconstructions over the last half millennium and model simulations confirm that volcanic forcing has induced a positive winter NAO response over northern Europe the first two winters after an eruption (Fischer et al. 2007), decadal-length annual and late winter (February–March) cooling over western (especially interior) North America (Wahl and Ammann 2010), and multidecadal variability of North Atlantic SSTs (Otterå et al. 2010).

The purpose of this paper is to provide an overview of the Last Millennium simulation of the Community Climate System Model, version 4 (CCSM4). We compare the LM simulation to data reconstructions of temperature, the hydrologic cycle, and modes of climate variability. We also include results, when available, from a previous simulation of the LM with version 1.4 of the National Center for Atmospheric Research (NCAR) Climate System Model (CSM 1.4; Ammann et al. 2007). The long (1300 yr) 1850 CCSM4 control simulation allows us to evaluate how the statistics of the climate modes have responded to the combined external forcings. For further discussion and analysis of the CCSM4 control simulation, the reader is referred to other papers in this special issue.

Section 2 describes the forcings datasets used in the CCSM4 LM simulation and section 3 gives a brief description of CCSM4 and improvements from CCSM3. Section 4 provides a comparison of the temperature and hydrologic responses of the CCSM4 LM simulation to the data reconstructions. Responses to volcanoes are presented in section 5. Section 6 discusses the primary modes of climate variability in the LM simulation, both in comparison to the data reconstructions and to the long CCSM4 control simulation. In section 7, we summarize the results and identify outstanding issues for future work.

2. Forcing datasets

The CCSM4 LM simulation starts at 850 and continues to 1850, where it matches up and is extended as an additional ensemble member of the CCSM4 twentieth-century simulations that end in December 2005. The forcings and boundary conditions for the LM simulation follow the protocols of PMIP3 (https://pmip3.lsce.ipsl.fr/wiki/doku.php/pmip3:design:lm:final) as discussed by Schmidt et al. (2012.) The extension of the LM simulation to 2005 adopts the same time-dependent datasets as the CCSM4 twentieth-century simulations. In addition, a second extension of the LM simulation to 2005 also included the incoming solar radiation changes associated with orbital variations, not included in the standard CCSM4 twentieth century completed for CMIP5. Time series plots of the forcing datasets are shown in Fig. 1.

For the LM volcanic forcing, we adopt the ice core–based index of Gao et al. (2008), which is based on volcanic deposition signals from 54 ice core records from both the Arctic and Antarctica. This reconstruction provides estimates of the stratospheric sulfate aerosol loadings from volcanic eruptions, modeled as a function of latitude, altitude, and month. The twentieth-century simulation uses an eruption dataset of similar temporal and spatial resolution as described by Ammann et al. (2003) and used in CMIP5 twentieth-century simulations. Stratospheric aerosols are prescribed in the model as a fixed single-size distribution in the three layers in the lower stratosphere above the tropopause. The LM contains a number of inferred volcanic eruptions estimated to be much larger than those that have occurred since 1850, in particular the 1258 eruption of unknown origin with estimated total sulfate aerosol injection into the stratosphere in excess of 250 Tg, as well as the Kuwae (1452) and Tambora (1815) eruptions. It should be noted that the timing and magnitude of the large volcanic eruptions vary among different reconstructions, depending on the screening processes for determining which are globally important eruptions. Several of the very large eruptions of the LM in the Gao et al. (2008) reconstruction have significantly smaller aerosol optical depths in the Crowley et al. (2008) alternate reconstruction for PMIP3.

Changes in total solar irradiance (TSI) are prescribed using the Vieira et al. (2011; hereafter VSK)

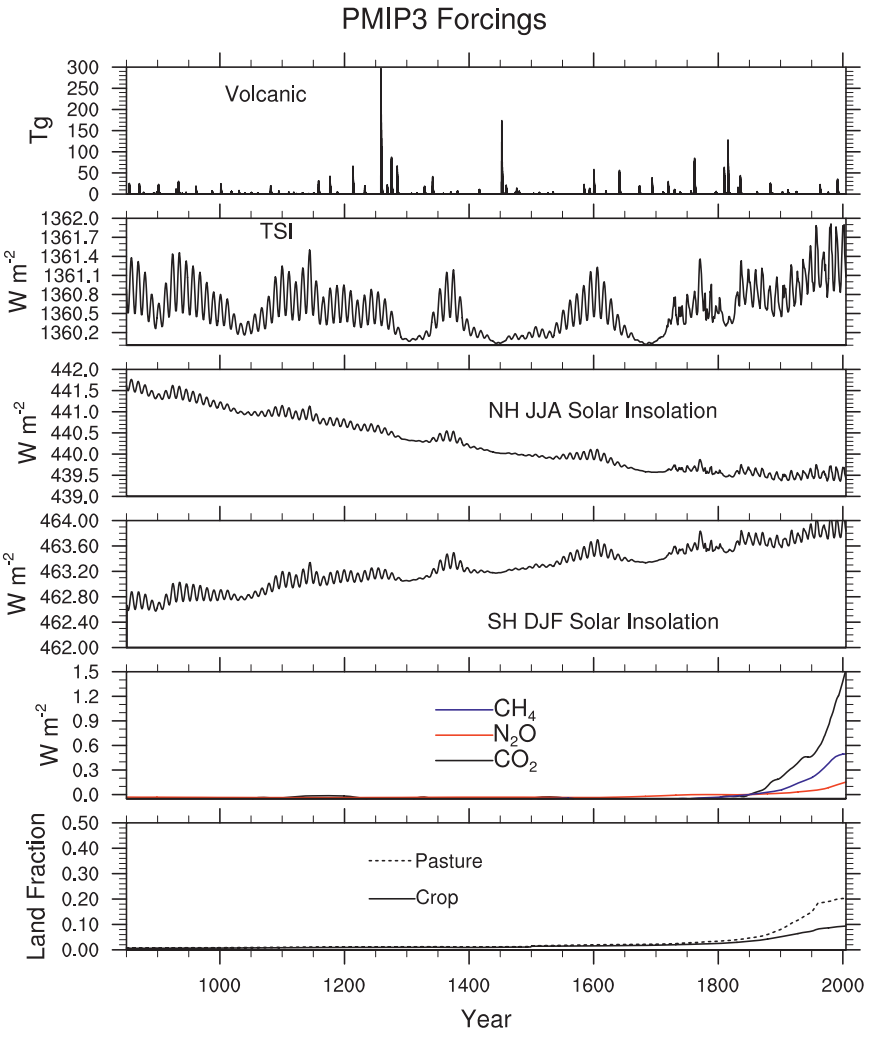

FIG. 1. Prescribed forcings used in the "Last Millennium" simulation and its extension through the twentieth century to 2005.

reconstruction merged to Lean (2009) at 1834 to have a smooth transition to twentieth-century CCSM simulations. The VSK reconstruction is based on physical modeling of the solar surface magnetic flux and its relationship with the isotopes. An estimated 11-yr solar cycle is superimposed on the VSK reconstruction as derived by Schmidt et al. (2012). The decrease in TSI at the Maunder Minimum as compared to modern times is ~0.1% (Schmidt et al. 2012). The CCSM4 simulations only consider the TSI with the variations derived from the reconstructions of VSK and Lean (2009) added to the 1360.9 W m^{-2} solar constant used in the 1850 control run. Solar-related ozone changes are not included in the LM simulation. Decadal to centennial solar variability is superimposed on the millennial trends in solar insolation associated with the orbital configuration changes over this period. Northern Hemisphere boreal summer insolation decreases by ~0.5% from 850 to 2005, while Southern Hemisphere (SH) austral summer insolation increases by ~0.2%.

The LM evolution of the concentrations of the principal long-lived greenhouse gases (GHGs; CO_2, CH_4, and N_2O) are imposed based on estimates from high-resolution ice cores in Antarctica [see Schmidt et al. (2012) for discussion and references]. Small variations from 850 to about 1800 are related to natural feedbacks in the carbon and nitrogen cycles. Post-1800, anthropogenic changes in these GHGs are apparent, with significantly increasing concentrations in the twentieth century to the end of the simulation at 2005. Aerosols, including sulfate, black and organic carbon, dust, and sea salt, are prescribed and non-time-varying with the same spatial distributions of the 1850 control simulation in the LM simulation. For the twentieth-century

extension, the time-varying aerosol datasets used in the CCSM4 twentieth-century simulations are used (Lamarque et al. 2010).

Anthropogenic changes to global land cover up until 1850 are relatively small; however, they can have regional influences important to compare to proxy records. Their importance—particularly in crops and pasture—increases as time approaches the start of the industrial era. In the LM simulation, we merged the Pongratz et al. (2008) reconstruction of land use, proposed by PMIP3, with that of Hurtt et al. (2009) used in the CCSM4 twentieth-century simulations to give a consistent and smoothly evolving land use change. The datasets are spliced together by scaling the Pongratz et al. (2008) dataset to match the Hurtt et al. (2009) dataset at 1500 for every land model grid point. The only plant functional types (PFTs) that are changed are those for crops and pasture; all other PFTs remain at their 1850 control prescription.

Results from the LM simulation are shown through 2005, where applicable, and include the LM extension that allows for orbital variations.

3. Model description

The Community Climate System Model is a general circulation climate model consisting of atmosphere, ocean, land, and sea ice component models that are linked through a coupler that exchanges state information and fluxes between components. The version used in this study, CCSM4, was released to the community in April 2010. The development of CCSM4 and a documentation of its 1850 control simulation can be found in Gent et al. (2011).

The LM simulation described in this paper uses the standard 1° version of CCSM4. Briefly, the atmospheric model is the Community Atmosphere Model, version 4 (CAM4), which uses the Lin–Rood finite volume core with a uniform resolution of 1.25° in latitude by 0.9° in longitude and 26 layers in the vertical (Neale et al. 2013). The land model is the Community Land Model, version 4 (CLM4), and adopts the same horizontal resolution as CAM4. As compared to previous versions, CLM4 includes an improved hydrology, land use capability, and a carbon–nitrogen biogeochemistry model that can impact the seasonal and interannual vegetation phenology (Lawrence et al. 2012).

The ocean model is based on the Parallel Ocean Program, version 2, of the Los Alamos National Laboratory (Smith et al. 2010). We use the standard ocean grid with a displaced grid North Pole, nominal 1° horizontal resolution (uniform 1.1° in longitude, variable in latitude from 0.27° at the equator to 0.54° at 33° latitude), and 60 levels in the vertical (Danabasoglu et al. 2012). CCSM4 includes changes in ocean physics and parameterizations that have significantly improved equatorial current structure, and reduced SST and sea surface salinity biases in the North Atlantic compared to CCSM3 (Danabasoglu et al. 2012).

The sea ice model is based on the Community Ice Code, version 4 (Hunke and Lipscomb 2008; Holland et al. 2012), and uses the same horizontal grid as the ocean component. The most notable improvement in the ice model is a new shortwave radiative transfer scheme that has resulted in much more reasonable and consistent surface albedos and radiative transfers in ice, melt ponds, and snowpack compared to CCSM3 (Holland et al. 2012). These improvements to the ice model have resulted in better simulation of Arctic ice thickness (Jahn et al. 2012). Mean Antarctic sea ice is more extensive in CCSM4 than in observations; however, the modeled variability compares well with observations (Landrum et al. 2012).

4. Surface temperature and precipitation evolution

a. Surface temperatures

The LM simulation shows a ''hockey stick''–like pattern in both the Northern and Southern Hemispheres, with cooling to the early 1800s of ~0.5°C (0.3°C) for the NH (SH) followed by warming to present (Figs. 2 and 3). NH (SH) surface temperatures warm by ~1.5°C (1.2°C) from 1850 to 2005, and ~1.4°C (1.0°C) in the twentieth century alone. The twentieth-century warming is overestimated in relation to the instrumental record, and is comparable to all CCSM4 twentieth-century simulations, which show too large a rate of heat gain after 1970 (Meehl et al. 2012). Much of this overestimation of heat gain is consistent with CCSM4 not including the negative forcing because of indirect effects of aerosols (Gent et al. 2011; Meehl et al. 2012). The equilibrium climate sensitivity of CCSM4 is 3.2°C, in the middle of the range of the CMIP3 models analyzed in the IPCC AR4 (Bitz et al. 2012). Simulated late-twentieth-century hemispheric surface temperatures are much warmer than the surface temperatures simulated during the MCA [defined in this paper as 950–1250, to be consistent with Mann et al. (2009)]. Overall the relative warmth exhibited by proxy temperature reconstructions during the MCA (centered around 1000) is somewhat damped in the NH in the LM simulation, particularly in terms of temporal extent into the eleventh and twelfth centuries. Strong cooling is associated with the large volcanic eruptions, with indications of multidecadal colder climate in response to larger eruptions, particularly when

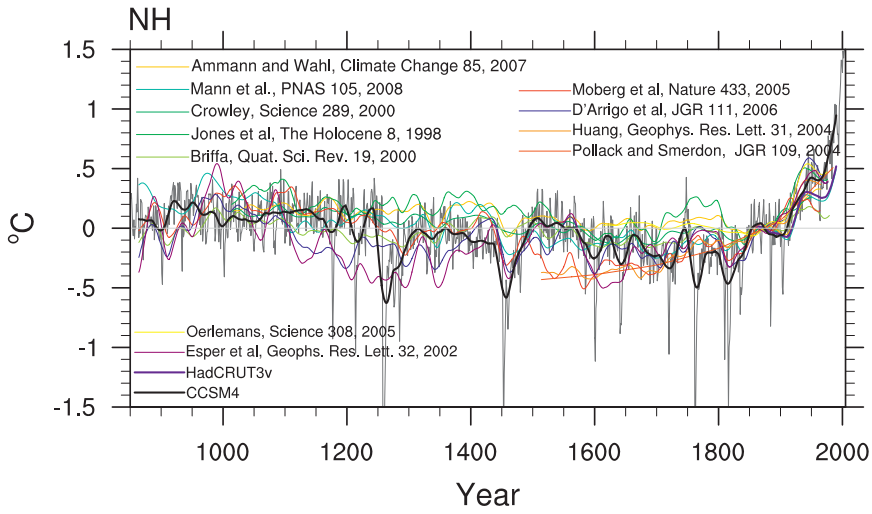

FIG. 2. Simulated NH annual mean temperature (light gray) shown as anomalies from the 1850–99 mean. The smoothed Gaussian-weighted (30 year) time series is plotted in black. Proxy-based reconstructions of NH temperature variations downloaded from the National Oceanic and Atmospheric Administration (NOAA) Paleoclimatology site (http://www.ncdc.noaa.gov/paleo/recons.html) are shown in colors.

the eruptions are decadally paced such as in the second half of the thirteenth century (cf. Briffa et al. 1998). This result is consistent with CCSM3, which displays a coupled sea ice–ocean feedback mechanism that can perpetuate the initial cooling from the direct effect of volcanic aerosols (Zhong et al. 2011). Twentieth-century simulations indicate that the CCSM4 response to volcanic eruptions is stronger than observed (Meehl et al. 2012).

The fact that greater cooling and warming trends are found in the NH than in the SH is an expected result due to the higher ocean-to-land ratio in the SH. The cooling trends are punctuated with even greater surface temperature drops associated with the explosive volcanic eruptions reconstructed for the LM. This is especially the case in the NH, where the model simulates cooling of ~1.0°–1.5°C after the large eruptions of the late thirteenth, mid-fifteenth, late eighteenth, and early nineteenth centuries, 2–3 times larger than the NH summer anomalies estimated from tree rings (Briffa et al. 1998), and even more so compared to multiproxy reconstructions of annual temperature anomalies [e.g., Wahl and

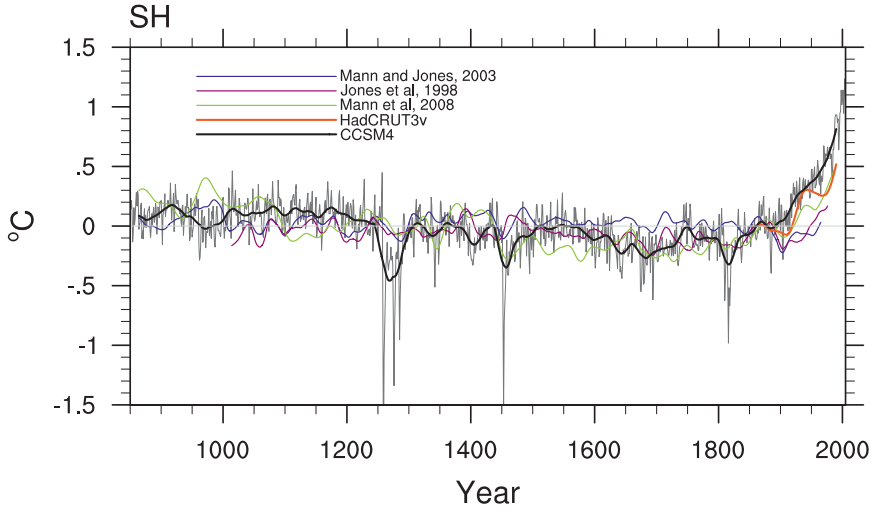

FIG. 3. As in Fig. 2, but for simulated SH annual mean temperature.

Ammann 2007; Moberg et al. 2005; cf. Mann et al. 2012 (for proposed reasons tree ring–derived paleoclimate information might underrepresent the amplitude of postvolcanic cooling)]. The NH cooling from the MCA peak to the early 1800s of ~0.5°C is in reasonable agreement with many of the published reconstructions shown in Fig. 2, although the temporal extent of peak MCA warmth is shorter. The relatively high-amplitude coolings reconstructed by Esper et al. (2002) and D'Arrigo et al. (2006) in the twelfth to fourteenth and seventeenth centuries and that reconstructed by Moberg et al. (2005) in the sixteenth and seventeenth centuries, which have received significant attention for this characteristic, are generally not supported by the LM simulation (exempting from consideration the possibly overstrong volcanic responses); it has been noted that the increased variability of NH reconstructions using extratropical tree-ring information (e.g., Esper et al. 2002) can potentially be explained by the spatial restriction of the proxy data used (Rutherford et al. 2005). Similarly, the simulated evolution of NH temperatures does not support the much higher-amplitude cooling (higher by a factor of ~2 for 50-yr smoothing of the time series) recently proposed by Christiansen and Ljundqvist (2011), using proxy data from extratropical, temperate, and high-latitude NH sites. The LM simulation also does not support relatively low-amplitude (less cool) reconstructions (e.g., Jones et al. 1998; Ammann and Wahl 2007; from the mid-thirteenth to the mid-nineteenth centuries). The preinstrumental SH time trajectory is in reasonable agreement with the smaller number of published reconstructions shown in Fig. 3.

Comparisons with recent regional summer reconstructions in the Arctic (Kaufman et al. 2009) and southern South America (Neukom et al. 2011) are shown in Fig. 4. The strong lowest-frequency (millennial scale) coherence of the simulated and reconstructed Arctic average temperature time series supports the inference by Kaufman et al. that the long-term decline into the early nineteenth century is driven by the orbital forcing reduction in NH boreal summer insolation. The LM simulation exhibits a positive linear relationship between NH summer temperature and boreal summer insolation (not shown), paralleling the relationship reported by Kaufman et al. for the Arctic (notably with significantly more variability in the relationship when the entire NH response to boreal insolation is considered). Summer Arctic temperatures simulated in the LM are consistently higher than the Kaufman et al. reconstruction during the MCA and twentieth century, possibly due to a polar amplification response discussed below. As with the larger hemispheric averages in relation to the instrumental record, twentieth-century (and earlier in the Arctic) temperatures are higher in the simulation than in the reconstruction.

The spatially limited reconstruction of Neukom et al. for southern South America (terrestrial area within 20°–65°S, 30°–80°W) has a similar overall temperature range for the millennium as the LM simulation (excepting the twentieth century), but the two time series differ significantly in terms of coherence or amplitude at multidecadal to centennial scales during much of the millennium. Given that there is much greater preinstrumental agreement between the SH millennial reconstructions and the simulated SH time series, it is possible that this disagreement may be an artifact of small-scale model offsets of relatively well-represented larger-scale circulation features that can have an amplified impact on averages in a relatively small target region. The spatial pattern reconstruction of Mann et al. (2009) shows this possibility for southern South America in relation to the LM simulation (cf. Fig. 7, described in greater detail below, and general discussion of spatial pattern results that follows).

The spatial pattern of simulated seasonal surface temperature differences between the MCA (950–1250) and the LIA (1400–1700) (Fig. 5) illustrates the expected polar amplification of the forced response (Holland and Bitz 2003), with more muted warming of the MCA relative to the LIA in the tropics as compared to higher latitudes. The differential warming is greatest at high latitudes of both hemispheres during their respective winters, indicating reduced seasonal contrast in the polar areas along with overall relative warming during the MCA in comparison to the LIA, which, if the case in the real world, may have been related to the persistence of high-latitude Norse settlements in Greenland during the MCA [but see McGovern (1991) for examination of the joint social and environmental conditions that appear to be involved in these settlement patterns]. The wintertime polar amplification of surface temperatures is associated with the large simulated reductions in sea ice during the MCA as compared to the LIA (Fig. 6). Higher summer insolation in the NH and spring insolation in the SH for the MCA as compared to the LIA allows more heating of the high-latitude oceans and less extensive and thinner sea ice going into the respective winter. The model also simulates enhanced MCA warming in boreal summer [June–August (JJA)] over the continents of North America, Europe, and Asia, regions where many of the long tree-ring proxy records are located (Jansen et al. 2007); see above concerning the extent to which some NH temperature reconstructions based on extratropical tree-ring data are not supported by the LM results for portions of the MCA.

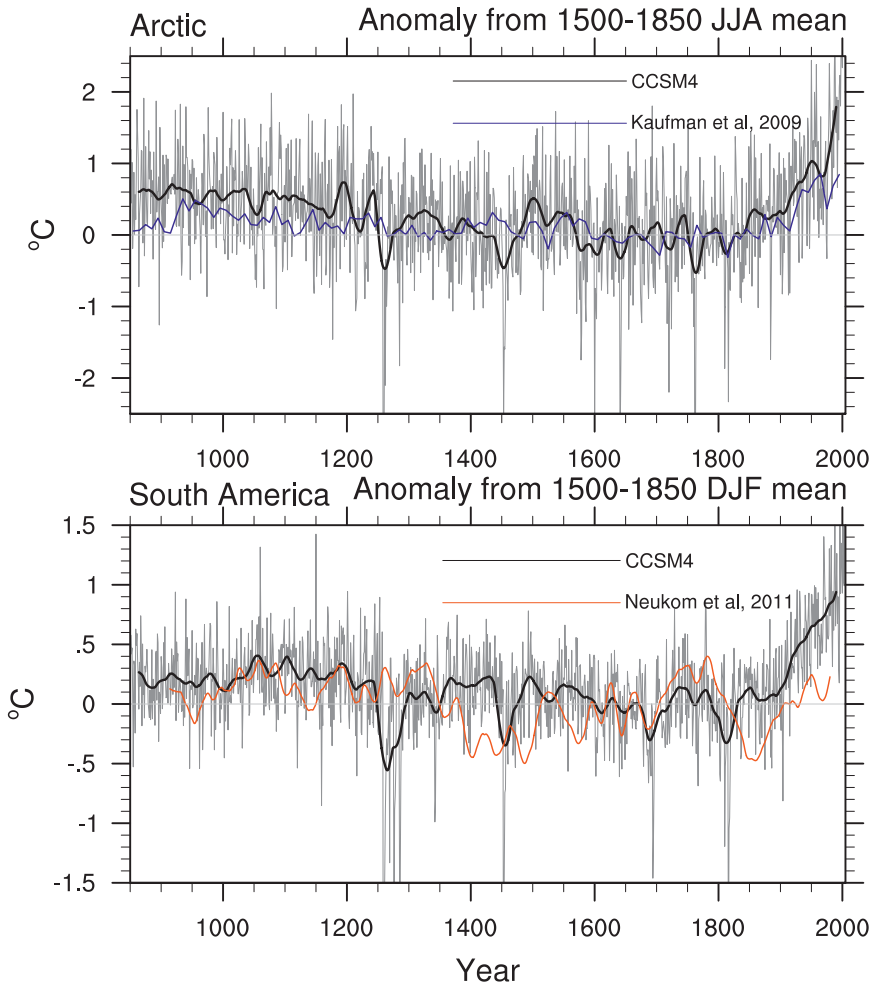

FIG. 4. Simulated Arctic Jun–Aug (JJA) and South American Dec–Feb (DJF) mean temperatures, shown as anomalies from the 1500–1899 mean along with proxy-based reconstructed temperatures. The proxy-based reconstruction's regional averages of land temperatures for the Arctic are poleward of 60°N (Kaufman et al. 2009) and for South America are 64.75°–19.75°S, 80.25°–30.25°W (Neukom et al. 2011).

Figure 7 shows detailed comparisons of the LM MCA-minus-LIA temperature difference CCSM4 map with comparable maps derived from the annual temperature reconstructions of Mann et al. (2009) and the last millennium medium and high solar forcing integrations of Ammann et al. (2007), developed with an earlier, lower-resolution (~3.75°) version of the CCSM (CSM 1.4). The polar amplification of the forced response is apparent in all the model results [cf. Mann et al. (2009) for comparison with the National Aeronautics and Space Administration (NASA) Goddard Institute for Space Studies Model E-R (GISS ER) model], and is also suggested by the reconstructed differences in central northwest North America, Iceland, northern Scandinavia and Russia, and far southern South America (generally the reconstructions do not extend into the very high latitudes; cf. Mann et al. 2009). The ''high solar'' [the ''high,'' ''medium,'' and ''low'' solar simulations of Ammann et al. (2007) refer to solar variability resulting from scaling the ^{10}Be record of Bard et al. (2000) such that the Maunder Minimum is reduced by 0.64%, 0.25%, and 0.1% respectively, compared to modern times] version of the CSM 1.4 runs shows an expected stronger differential between the MCA and LIA in comparison with the ''medium solar'' version; in the ''low solar'' CCSM4 LM simulation the differential strength is closer overall to the CSM 1.4 medium solar version, but with stronger warm anomalies in the polar and NH interior continental regions. The reconstructed differentials show much more spatial variability than the model runs, in particular indicating significant cooling in the equatorial Pacific, subtropical Indian, and southern

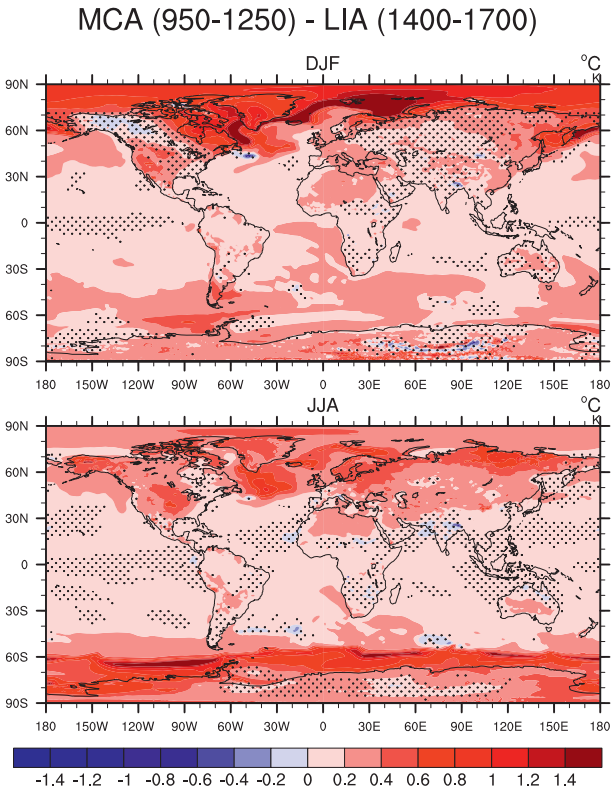

FIG. 5. CCSM4-simulated surface temperature anomalies, Medieval Climate Anomaly (MCA; defined as 950–1250) minus Little Ice Age (LIA; defined as 1400–1700), for (top) DJF and (bottom) JJA. Regions with anomaly confidence at <95% are stippled in black.

Pacific Oceans, and in South America, western Africa, southeastern Australia, and interior and Southeast Asia. It should be noted that the relative coherence of hemispheric mean values between the LM simulation and the reconstructions occurs even as some of the regional details do not because the regional differences in the reconstructions are averaged out at the hemispheric level, and also because the relatively cool MCA contribution of the tropics in the eastern central Pacific would be offset by relative MCA warming in other portions of the tropics, particularly the tropical Atlantic.

Notably, the model simulations do not indicate the La Niña–like average cooling reconstructed by Mann et al. (2009) in the eastern Pacific during the MCA relative to the LIA, which has also been suggested by other proxy-based evidence [Cobb et al. 2003; cf. Graham et al. 2011 (for a summary)] as well as model experiments, albeit driven by very large surface shortwave heat flux into the western Pacific and tropical Indian Ocean that resulted in anomalously warm SSTs in these regions (Graham et al. 2011). Such an average tendency toward ENSO cool-state conditions during the MCA has also been associated with a tendency toward positive-phase North Atlantic Oscillation (NAO) pressure conditions (Trouet et al. 2009; Graham et al. 2011) during NH winter, in conjunction with the potential for a similar North Atlantic pressure pattern and high pressure ridging/drought conditions in summer in interior central North America (Wahl et al. 2011). It should be noted that present-day observations only show very weak correlations between the winter NAO index and Niño-3.4. As noted in section 6, the LM simulation indicates, at most, only the hint of a tendency toward a positive average NAO state during the MCA, which, according to the results of Trouet et al. (2009), Graham et al. (2011), and Wahl et al. (2011), is potentially consistent with the lack of tendency toward a La Niña–like state during the MCA in the LM output. One clear distinction between the model generations is that the CCSM4 simulation does not indicate the cool temperatures during the MCA in the North Atlantic and Labrador Sea that occur in the most comparable (medium solar) version of the CSM 1.4 runs. This lack of cooling is consistent with the reconstructions, although the positive difference is much weaker in the reconstructions compared to the LM simulation.

b. *Hydroclimate*

Unlike simulated surface temperature changes, the LM simulated changes in seasonal and annual precipitation-minus-evaporation ($P-E$) between the MCA and the LIA are not statistically significant (within the natural inherent variability of the model using the Student's t test) except in a few locations in Greenland, Central and South America, and North America. The LM simulation indicates enhanced winter MCA moisture over most of southern and western Greenland, which is related to the reduced sea ice extent simulated in adjacent portions of the North Atlantic and the polar amplification of relative MCA warming, especially in winter. The model also simulates MCA boreal winter dryness extending from Panama to Venezuela consistent with a speleothem record from southern Panama (Lachniet et al. 2004), but not with the interpretation of the Cariaco basin record (Haug et al. 2001).

Over North America the LM simulation has statistically significant (at the 80% confidence level) winter $P-E$ changes, drier in the southwestern United States and wetter in the Pacific Northwest and northeastern Canada during the MCA relative to the LIA (Fig. 8). Terrestrial proxy records in the western United States indicate a MCA climate that was marked by arid conditions and elevated incidence of wildfires (dots in Fig. 8). These records have been interpreted as primarily indicative of decreases in winter-half precipitation and include multidecadal periods of more severe regional

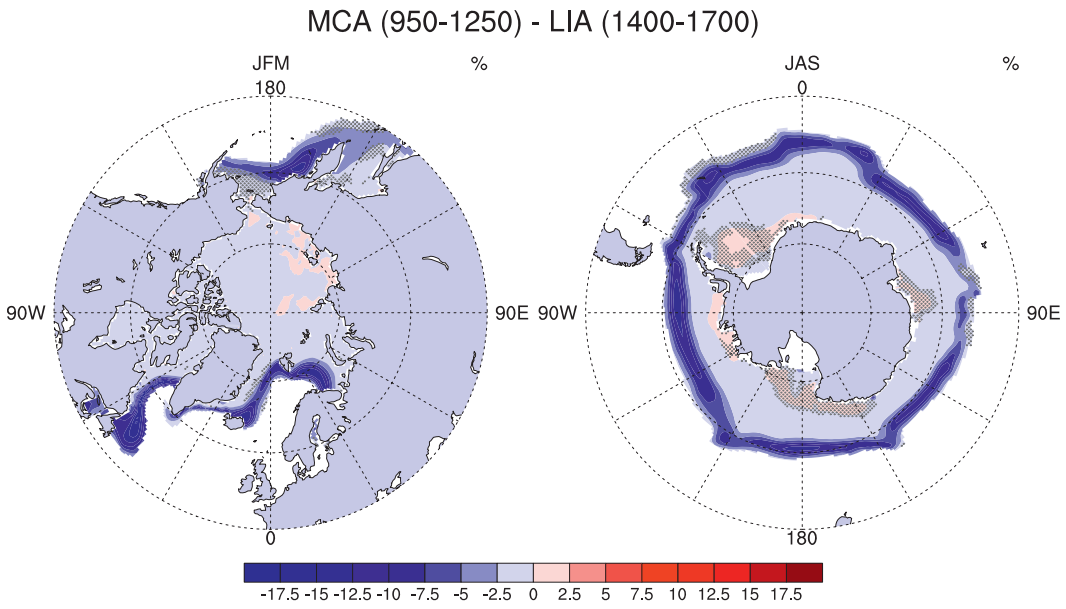

FIG. 6. Simulated sea ice concentration anomalies, MCA minus LIA, for (left) Jan–Mar (JFM) and (right) Jul–Sep (JAS). Differences significant at <95% are stippled in gray.

droughts with inferred precipitation decreases of 15%–25% or more (Graham et al. 2007). Southwestern United States precipitation simulated by the model decreases by ~10%–15% for the 300-yr MCA average as compared to the LIA, although it is highly variable with multidecadal dry and wet periods. The single-site proxy data additionally suggest the simulated boundary between winter wet and dry conditions in western North America, and possibly the entire regional moisture pattern, is spatially offset somewhat southeastward of their true MCA position. The LM simulation has statistically significant summer changes toward drier conditions in the central United States during the MCA relative to the LIA, consistent with bog and lake records (Fig. 8).

The effective moisture available for plant growth in CCSM4 can be evaluated using the simulated water availability factor β_t which relates soil moisture conditions to soil moisture stress on plant photosynthesis and transpiration (Lawrence et al. 2007). The factor β_t can range between 0 (at wilting point potential) and 1 (at saturated soil matric potential). This simulated variable allows for intraseasonal memory of precipitation departures from one season to the next, providing a model measure to compare to the continentwide gridded summer Palmer Drought Stress Index (PDSI) maps [Cook et al. 2004b; Cook 2008; known as the *North American Drought Atlas* (*NADA*)], which are the most strongly validated reconstructions of their kind (cf. Cook et al. 2010; Wahl and Morrill 2010). The simulated pattern of reduced soil water availability over the United States during boreal summer is in general agreement with the NADA reconstruction (Fig. 8). This reduction is most pronounced in central North America.

Observational studies of North American megadroughts (Seager et al. 2007a; Conroy et al. 2009) and modeling analyses (Schubert et al. 2009; Burgman et al. 2010) indicate that reduced precipitation and the longest and most persistent droughts over the United States in the last 1200 years can be explained by a pattern of cold eastern equatorial Pacific SSTs. The seasonal pattern of decreased model $P-E$ over the southwestern United States and enhanced moisture in the Pacific Northwest in winter during the MCA relative to the LIA is reminiscent of modern teleconnections during La Niña events (Seager et al. 2007a), even though the model does not exhibit La Niña–like relative MCA cooling in the equatorial Pacific and La Niña–like circulation changes are not sufficient to explain many proxy-reconstructed climate changes during the MCA (Graham et al. 2011). Climate projections of the twenty-first century also show regional drying (Solomon et al. 2007), although the IPCC AR4 models vary with regard to a trend toward La Niña conditions (Seager et al. 2007b).

A positive Atlantic multidecadal oscillation (AMO) and the North Atlantic SST anomalies associated with this mode of variability have been associated with drought over the central United States (Enfield et al. 2001; Feng et al. 2011; Oglesby et al. 2011; Nigam et al. 2011). Modeling studies point to the subtropical SST anomalies

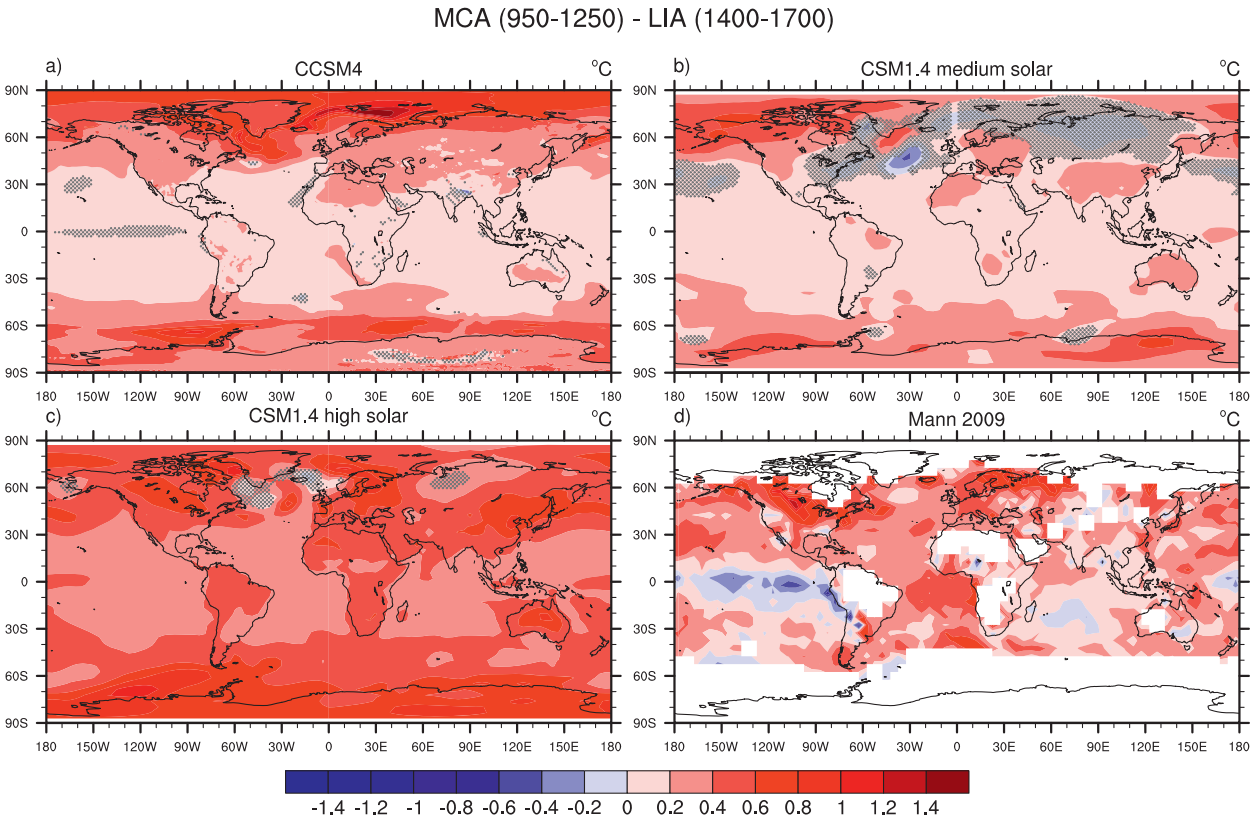

FIG. 7. Simulated annual surface temperature anomalies, MCA-minus-LIA, for (a) CCSM4, (b) CSM 1.4 medium solar run, (c) CSM 1.4 high solar run, and (d) Mann et al. (2009) proxy-based reconstruction. Differences significant at <95% are stippled in gray. Uncertainties in the reconstruction are discussed in Mann et al. (2009).

associated with this mode as important for the summer continental drying (Schubert et al. 2004; Sutton and Hodson 2005; Kushnir et al. 2010), and that the largest precipitation response tends to occur when the Pacific and Atlantic have SST anomalies of opposite sign (McCabe et al. 2004; Seager et al. 2007a; Schubert et al. 2009). Observational studies for the twentieth-century Great Basin droughts, on the other hand, find an important role for SST anomalies in the North Atlantic subpolar gyre (Nigam et al. 2011). The simulated AMO (defined and discussed in section 6 below) was positive (negative) throughout most of the MCA (LIA). The largest MCA and LIA mean North Atlantic SST anomalies occur in the northern basin, with much smaller mean SST changes in the subtropical North Atlantic.

5. Volcanic responses

To further assess whether the global and hemispheric cooling responses of CCSM4 for the large eruptions of the LM are realistic, we examine the postevent spatial patterns and also compare them to the regional postevent reconstructions of Fischer et al. (2007), Wahl and Ammann (2010), and Anchukaitis et al. (2010). For consistency, we compare the model response to eruptions from 1500 to 1850, the time period jointly covered by the proxy reconstructions. Superposed epoch analysis (SEA; see Adams et al. 2003) is used to show the model response to volcanic forcing. We define a large volcanic event as one that emits sufficient aerosols to result in a decrease in the clear-sky net solar flux at the top of the atmosphere by 2 W m^{-2} or more from the 10-yr running mean. Ten events between 1500 and 1850 meet this criterion. We use a 21-yr window for the SEA; this response is shown as a deviation from the 10-yr mean prior to an event. Year 0 of an eruption is defined as the first year (annual) after an eruption or the first season at least 3 months after the peak eruption—sufficient time for sulfur dioxide (SO_2) to be converted into sulfate aerosols (e.g., Zhao et al. 1995), and for the aerosols to be globally redistributed in the atmosphere.

Figure 9 shows the December–February (DJF) spatial postvolcanic SEA composite results for years 0–3 for the equatorial Pacific Ocean. A weak El Niño–like SST pattern occurs in the first year after the event (Fig. 9a), changing to more La Niña–like conditions along the

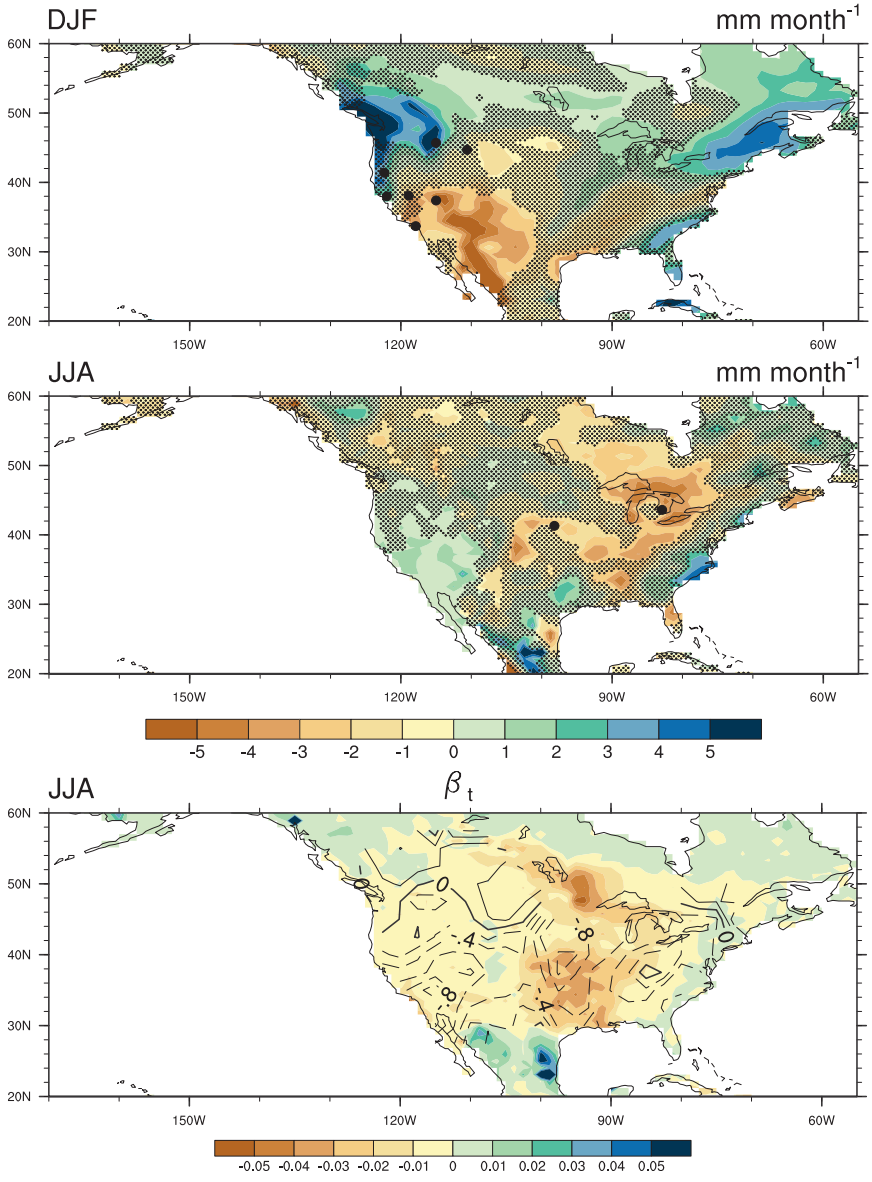

FIG. 8. Simulated North American $P-E$ anomalies, MCA minus LIA, for (top) DJF and (middle) JJA. Differences significant at <80% are stippled in gray. Locations of dry medieval conditions summarized by Cook et al. (2004b) and Graham et al. (2007) and suggested by charcoal (Millspaugh et al. 2000; Mohr et al. 2000), marsh and lake salinities (Byrne et al. 2001; Laird et al. 1996), pollen records (Davis 2002; Wigand 1997; Wigand and Rhode 2002), lake sediments (Brunelle and Whitlock 2003), and bog peat cores (Booth and Jackson 2003) are shown by black circles. (bottom) Simulated anomalies, MCA minus LIA, of the soil availability factor for JJA (color fill). Contours of tree-ring based summer Palmer Drought Severity Index (PDSI) for the MCA from Cook et al. (2008) are overlaid with positive (negative) values indicated by solid (dashed) lines.

equator (but not as much away from the equator) in the second and third years (Figs. 9b,c). By the fourth post-event year, the SEA SST anomalies in most of the region are small (Fig. 9d). This general temporal sequence (an initial El Niño–like response changing to a secondary La Niña–like response) is consistent with at least some observational studies [e.g., Adams et al. 2003; D'Arrigo et al. 2009 ("TexMex" reconstruction); Wilson et al. 2010] although there are also inconsistencies in the observational studies (cf. Wilson et al. 2010). Similar results are reported in modeling studies using a less complex model platform that realistically simulates

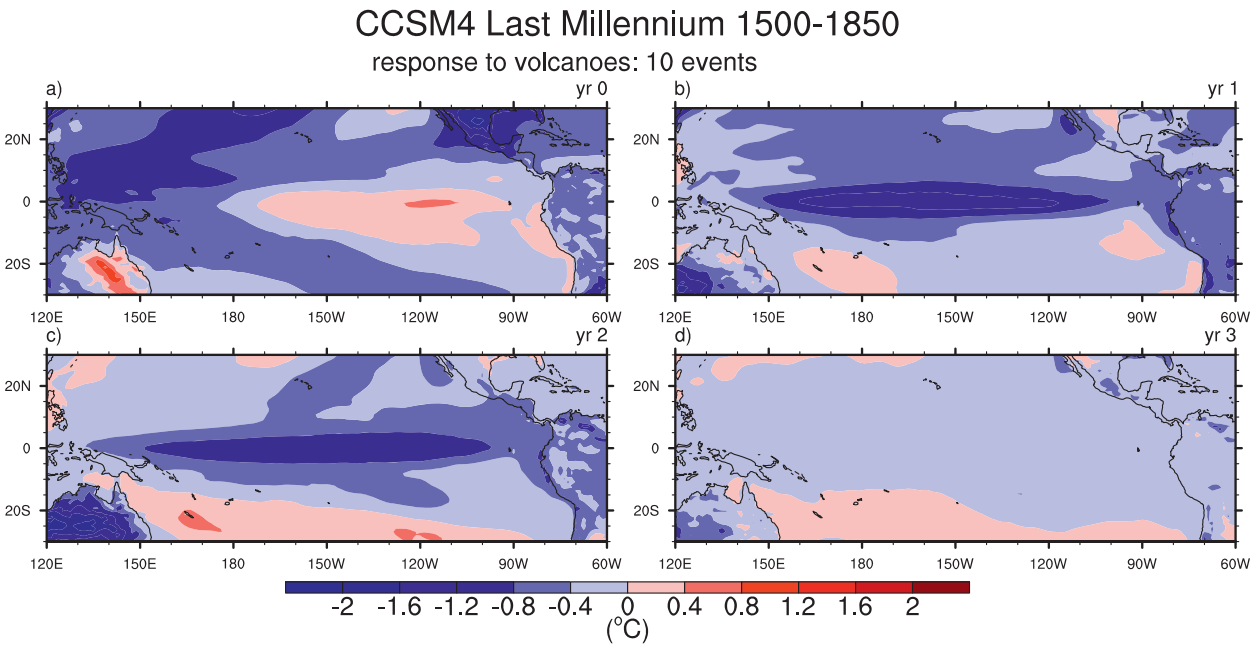

FIG. 9. Superposed epoch analysis (SEA) CCSM4 composite responses of the equatorial Pacific DJF SSTs to 10 volcanic events, 1500–1850, years (a) 0, (b) 1, (c) 2, and (d) 3 (see text for method).

ENSO behavior (Mann et al. 2005; Emile-Geay et al. 2008); thus, the LM simulation potentially broadly supports the dynamic interpretations suggested by these studies (but compare the more complex nature of matches and mismatches with region-specific postvolcanic responses described below).

Figure 10 shows a comparison of the postvolcanic response in the LM simulations with results from proxy-derived temperature reconstructions in temperate western North America [Wahl and Smerdon 2012 (see their auxiliary material); Wahl and Ammann 2010]. The SEA composite February–March (FM) response reconstructed

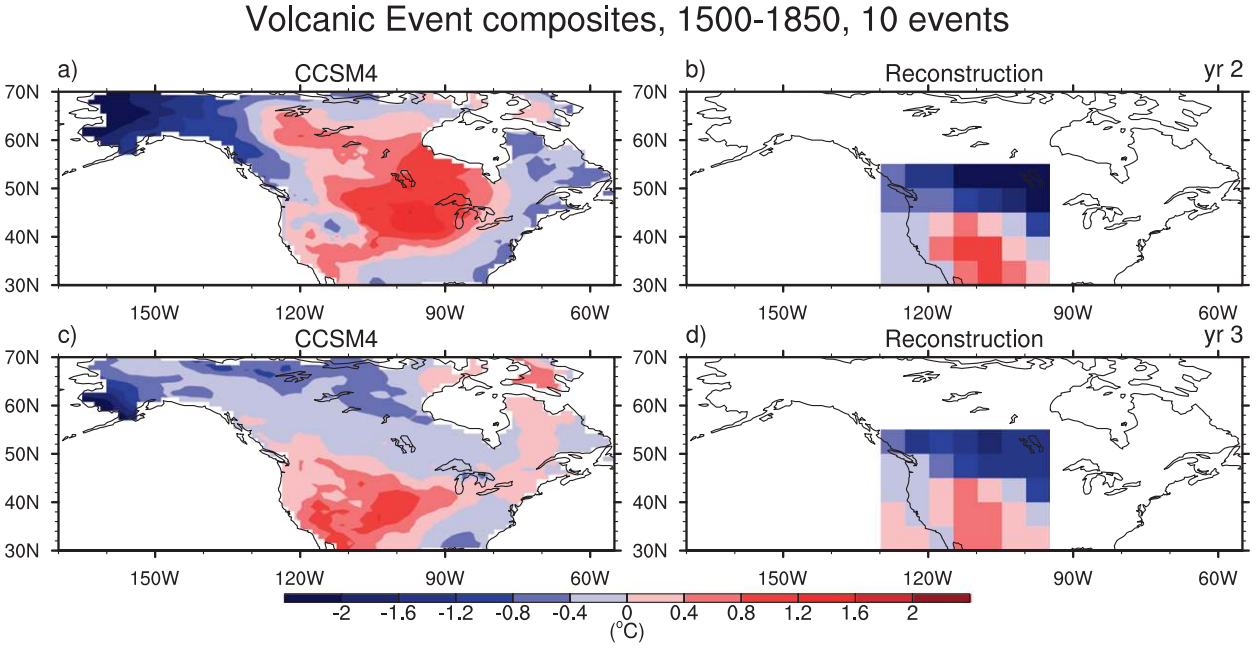

FIG. 10. SEA composite responses of North American Feb–Mar (FM) surface temperatures to 10 volcanic events, 1500–1850, years 2 and 3, for the (a),(c) CCSM4 Last Millennium, and (b),(d) proxy-based reconstruction of Wahl and Ammann (2010).

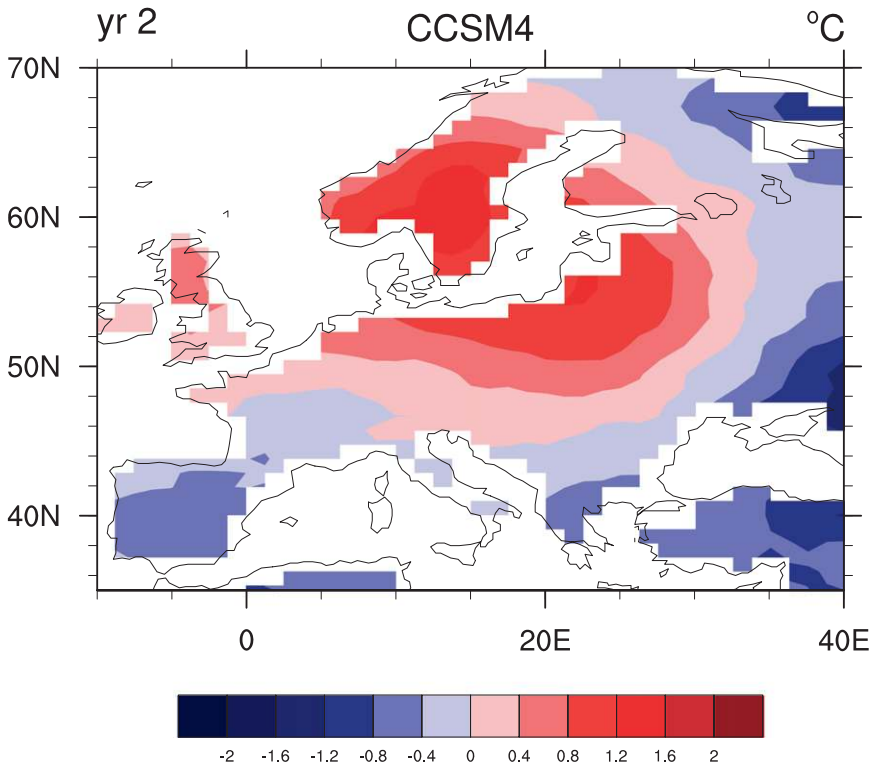

FIG. 11. SEA composite responses of European winter (DJF) surface temperatures to 10 volcanic events, 1500–1850, year 2 for the CCSM4 Last Millennium simulation.

in western North America for the third and fourth postevent years (Figs. 10b,d) indicates a La Niña–like pattern, consistent with the ''cool season''-calibrated Niño-3.4 reconstructions reported in D'Arrigo et al. (2009; ''TEXMEX'') and Wilson et al. (2010; ''TEXMEX'' and ''MANN''), especially for the latter year. This pattern is highlighted by warming in the interior Southwest and distinct cooling north of this that becomes particularly sharp in the midcontinent (cf. with the modeled temperature pattern forecast for a La Niña winter; http://www.noaanews.noaa.gov/stories2011/20111020_winteroutlook.html, accessed 17 December 2011). The simulated regional SEA pattern for the third postevent year (Fig. 10a) is dissimilar to the reconstructed pattern (Fig. 10b), even though the indication of La Niña–like conditions in the reconstruction is matched by the simulated equatorial Pacific conditions (Fig. 9c). In contrast, the simulation exhibits a broadly comparable SEA pattern for the fourth postevent year (Fig. 10c), including the relatively zonal gradient from northwest to southeast between southern warming and northern cooling (Fig. 10d), even though La Niña–like conditions have essentially dissipated in the equatorial Pacific by this time (Fig. 9d). The entire simulated pattern is shifted northward compared to the reconstructions and the reconstructed enhanced midcontinent cooling does not occur in the model. This shifting of spatial pattern is reminiscent, although opposite in direction, to that seen in the continental winter MCA–LIA hydrological patterns for western North America discussed above, and it highlights the difficulty of applying (even fine scale) simulation results to questions of patterns of forced response at the scale of a few degrees of latitude/longitude. This complex combination of matches and mismatches with the regional reconstruction data represents a notable area for further research beyond the scope of this paper.

For the 10 large eruptions after 1500 —which are assumed to be tropical eruptions, although some, particularly in the eighteenth century, do not match those identified by Fischer et al. (2007)—CCSM4 simulates summer surface temperature cooling (not shown) in Europe similar to proxy reconstructions. CCSM4 captures the dynamically induced pattern of winter warming over northern Europe and Scandinavia and cooling over southern Europe reconstructed by Fischer et al. (Fig. 11), although the timing of the model response is again offset. In comparing the simulated versus reconstructed postvolcanic SEA response in Europe, there is a clear match between the winter patterns for the model's third postevent

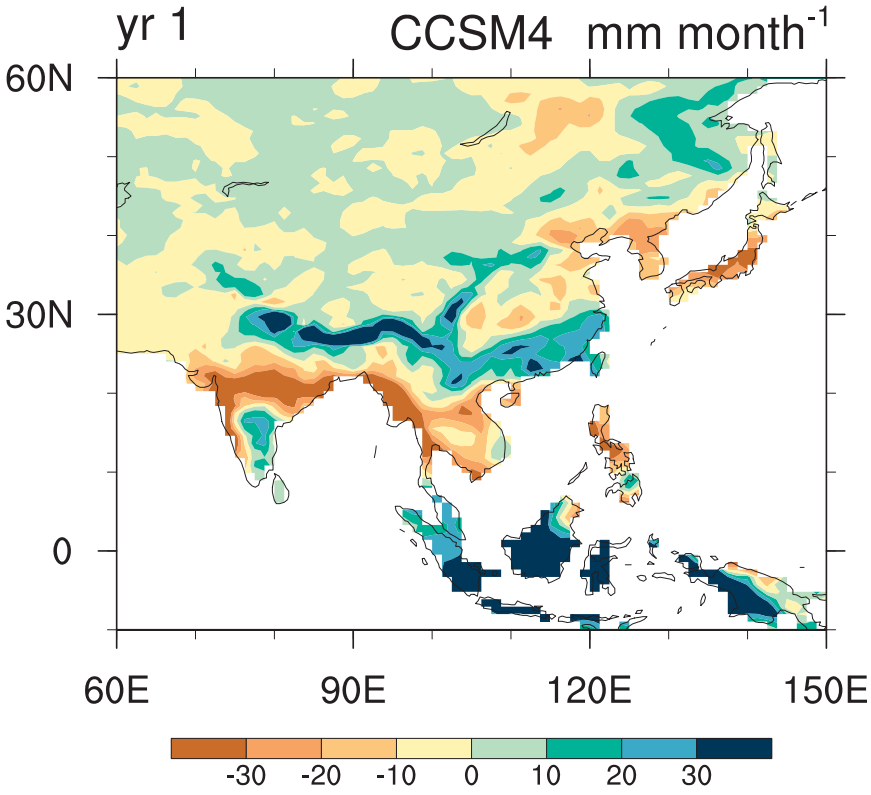

FIG. 12. SEA composite responses of Asian summer (JJA) precipitation minus evaporation ($P-E$) to 10 volcanic events, 1500–1850, year 1 for the CCSM4 Last Millennium simulation.

year and the reconstructed second postevent year, but not for simultaneous time periods.

For the 10 large eruptions post-1500, CCSM4 simulates drying in Southeast Asia, India, and northeast China during both the first and second postevent year (Fig. 12) (associated with a weakening of the Asian monsoon). This pattern closely follows observed anomalies of precipitation, runoff, and PDSI found for the first year after the Pinatubo eruption in June 1991, after adjusting for the effects of El Niño during 1992 (Trenberth and Dai 2007). Similar hydrological responses to tropical eruptions were found in a previous version of CCSM (Schneider et al. 2009; Anchukaitis et al. 2010) as well as the GISS model (Oman et al. 2005). Proxy reconstructions, on the other hand, suggest nearly opposite anomalies in PDSI in the Asian monsoon region (Anchukaitis et al. 2010). Possible reasons for this disagreement are discussed by Anchukaitis et al. (2010).

6. Modes of climate variability

The dominant climate modes of variability have been shown to have considerable influence on regional temperature and precipitation variations on seasonal to multidecadal time scales. Questions remain as to whether the short instrumental records adequately represent the full range of behavior of these modes. Did the periods and magnitudes of the dominant climate modes change in the past and, importantly, will they change in the future? Here, we present the 1000-yr simulation of the LM in comparison to the 1850 control simulation to study whether or not changes to internal modes of variability of ENSO, PDO, NAO, and AMO occur as a result of external forcings. The simulated modal indices are compared to those reconstructed from paleorecords, which have either be estimated directly as from coral records in the Pacific for ENSO (e.g., Cobb et al. 2003) or, more often, indirectly reconstructed using proxies that record teleconnection patterns of temperature and/or precipitation associated with a climate oscillation (e.g., MacDonald and Case 2005; Trouet et al. 2009; Li et al. 2011).

a. Pacific modes: ENSO and PDO

The El Niño–Southern Oscillation, with a time scale of 2–7 years, is a coupled ocean–atmosphere fluctuation in the tropical Pacific with impacts on worldwide seasonal weather. It is evident as the leading-order EOF of

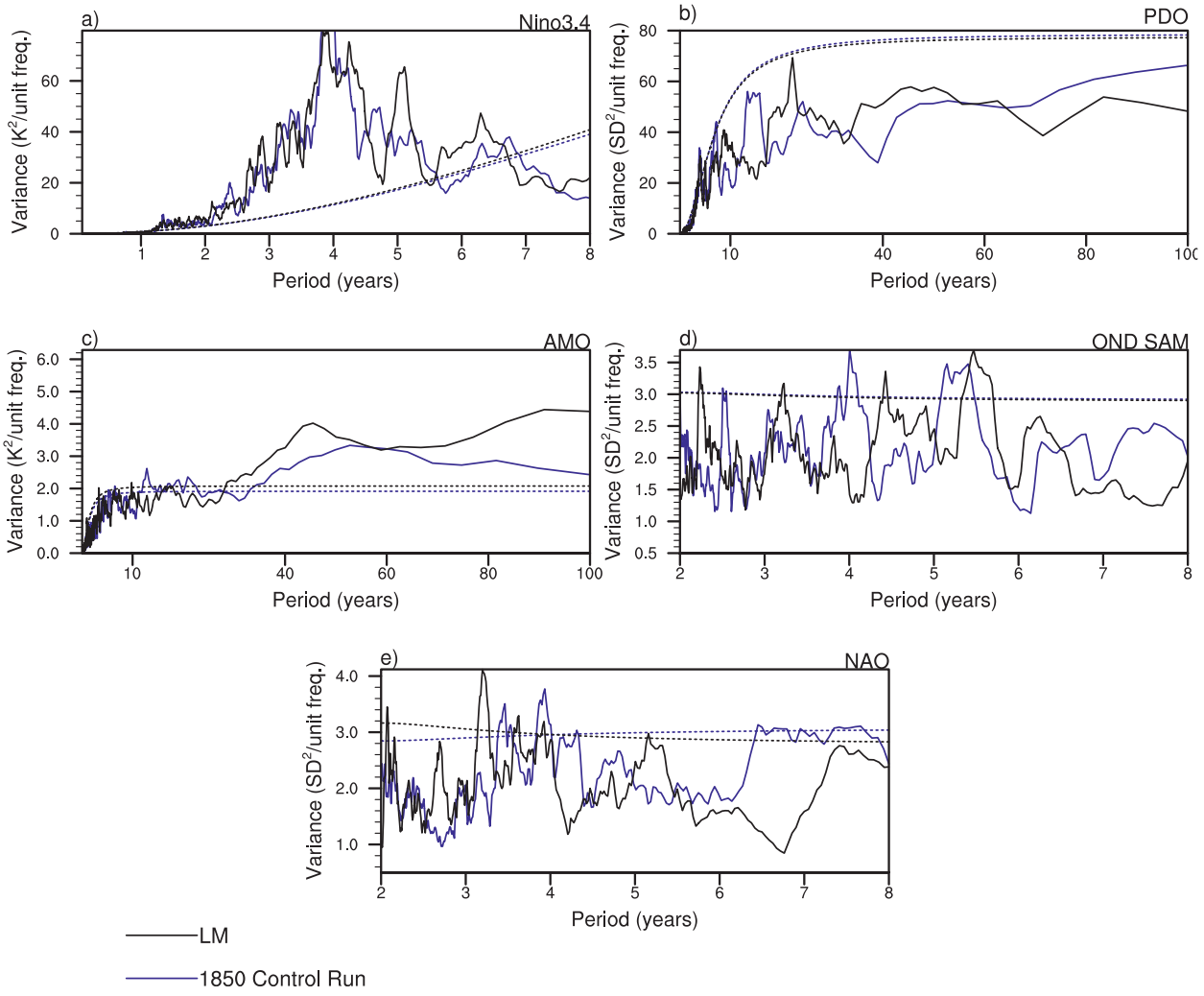

FIG. 13. Comparison of the spectrums of the modes of variability: the (a) Niño-3.4, (b) PDO, (c) AMO, (d) Oct–Dec (OND) southern annular mode (SAM), and (e) NAO for the LM simulation (black) and the 1850 control simulation (blue). Dashed lines (black/blue) indicate 95% confidence level (LM/1850 control run).

monthly sea surface temperature (Deser et al. 2012). The regional effects of ENSO, which tend to be opposite between El Niño (the warm phase) and La Niña (the cool phase) include droughts/floods in the western Pacific, increased/decreased rainfall in the southwest United States and Peru, weaker/stronger Indian monsoons, and warmer/cooler temperatures in northwestern North America.

ENSO dynamics are significantly improved in CCSM4 compared with CCSM3, including a longer period of 3–6 years and increased duration of La Niña compared with El Niño although the magnitude of ENSO in CCSM4 is about 30% greater than in observations (Deser et al. 2012). Improvements in the ENSO frequency distribution are related to improvements in the deep convection parameterization in CAM (Richter and Rasch 2008; Neale et al. 2008). The global teleconnections for temperature and precipitation are also generally well simulated.

In this paper, we use the Niño-3.4 index (the area weighted monthly SST from 5°S to 5°N and 120° to 170°W after removing the long term monthly means) as an indicator for ENSO. ENSO in the LM simulation shows an amplitude and power spectrum (greatest variance in the 3–7-yr periods) similar to both the instrumental record and the CCSM4 1850 control simulation (Figs. 13 and 14). The Niño-3.4 of the LM simulation has a slightly higher variance (1.20°C^2 for 850–1850) than the control run (1.10°C^2 for years 404–1300), suggesting a small increase in magnitude due to the transient forcings. Although the dominant ENSO variability throughout the LM occurs at the 3–7-yr periods, wavelet

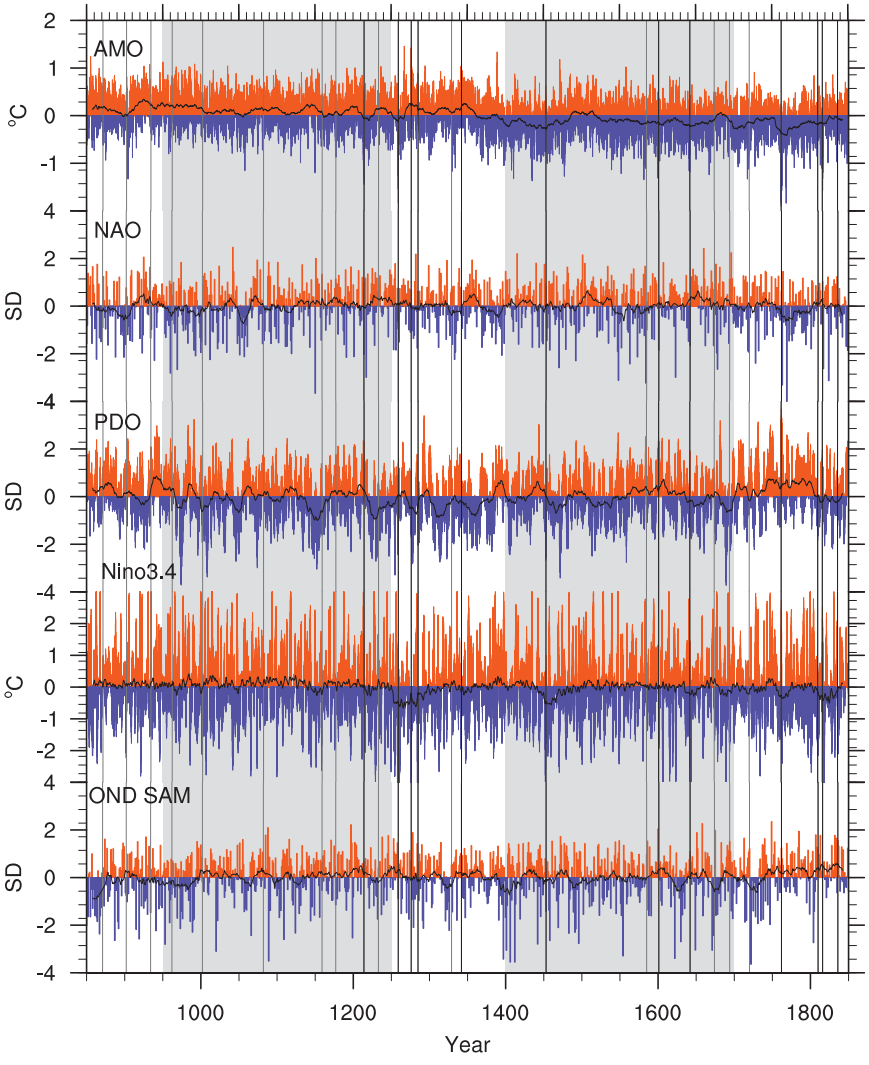

FIG. 14. Simulated time series of selected modes of variability: AMO, NAO, PDO, Niño-3.4, and OND SAM. Annual time series filtered by 16-yr running average are shown by black curves. Gray shading indicates MCA (950–1250) and LIA (1400–1700). Black and gray vertical lines give years of major explosive volcanic eruptions (defined as sufficient to reduce clear-sky net solar flux at the top of the atmosphere by 5 and 2 W m^{-2} from the 10-yr running mean, respectively). AMO and Niño-3.4 are plotted in original units of degrees Celsius; all other indices are normalized over the length of the time series (850–1850) and plotted in units of standard deviation.

analysis of the LM simulation (not shown) indicates enhanced Niño-3.4 variability at centennial time scales not present in the long control run. This enhanced variability occurs during the time period of enhanced large tropical eruptions from 1250 to 1500, suggesting a possible role for volcanic forcing on these longer time scales in addition to the short-term response within the first few years after an eruption (see section 5). Dating uncertainties in Niño-3.4 reconstructions have precluded testing a volcanic correlation in the data at this longer time scale (McGregor et al. 2010; Emile-Geay et al. 2013). Niño-3.4 reconstructions back to 1200 suggest a consistent centennial-scale inverse relationship between Niño-3.4 and solar irradiance reconstructions (Emile-Geay et al. 2013). This correlation, though, is only significant when calculated for large-amplitude solar reconstructions but is inconclusive when a small-amplitude solar forcing reconstruction similar to that in our LM simulation is used. Future CCSM4 single-forcing simulations with volcanic and different solar forcing histories are needed to further assess this relationship in CCSM4.

The first reconstructions of ENSO for the LM were based on historical evidence, such as ship and military

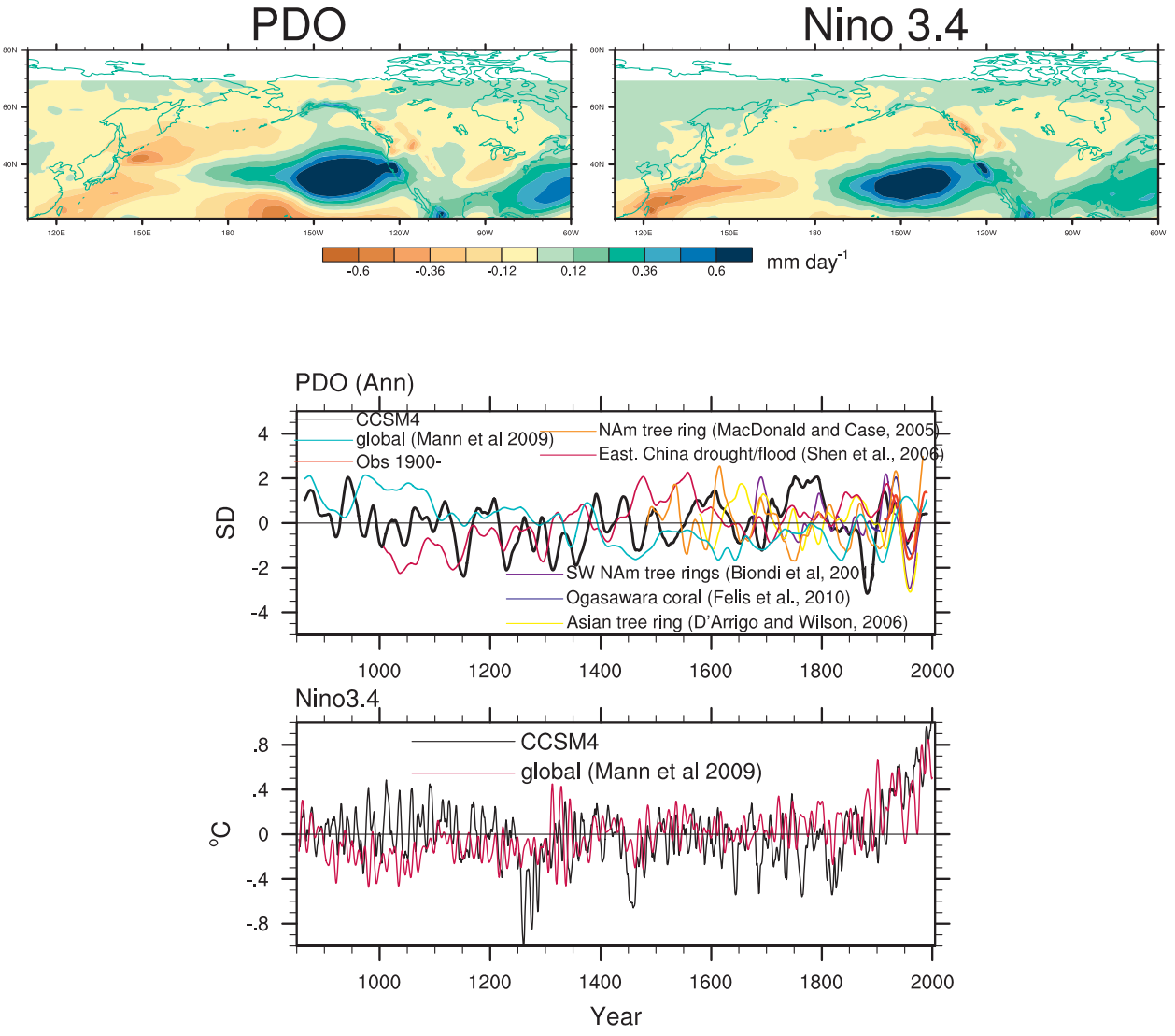

FIG. 15. Regressions of boreal winter Dec–Mar (DJFM) precipitation on the (top left) PDO and (top right) Niño-3.4 in the CCSM4 LM simulation, and time series of the (middle) PDO and (bottom) Niño-3.4. Annual PDO time series are first smoothed (30-yr Gaussian weighted) and then standardized over the entire time series (z score over 850–2005, or over the entire length of the individual time series for those proxy-based reconstructions that span a shorter time period). Niño-3.4 series are smoothed (10-yr Gaussian weighted) and are plotted as anomalies from the mean in degrees Celsius. CCSM4 LM is shown in black. Proxy-based reconstructions are shown in colors.

records, and confined to occurrences of strong El Niños (Quinn et al. 1987). Subsequently, ENSO reconstructions have been extended back to cover more of the LM and to include the full range of ENSO variability, using coral records in the equatorial Pacific core regions of ENSO SST variations (Dunbar et al. 1994; Cobb et al. 2003), as well as proxies such as tree rings and ice cores, which record more remote impacts of ENSO on regional temperatures and precipitation (Stahle et al. 1998; Braganza et al. 2009; D'Arrigo et al. 2009: Li et al. 2011). A proxy ENSO reconstruction that combines the common signals of 10 different ENSO proxy reconstructions into one reconstruction has been recently been constructed to filter out differences unrelated to nonclimatic factors influencing the proxy (McGregor et al. 2010). This unified ENSO proxy reconstructions indicates enhanced ENSO variance during the twentieth century as compared to the period from 1660 to 1880. The Mann et al. (2009) reconstruction also shows greater Niño-3.4 variance during the twentieth century, a feature not simulated by CCSM4 (Fig. 15). The Palmyra Island coral records also show more intense ENSO variability during

the mid-seventeenth century (Cobb et al. 2003). Both studies conclude that ENSO variability over the LM is primarily associated with internal dynamics rather than external forcings, a result also found in the CCSM4-simulated Niño-3.4 from 850 to 1850 (Fig. 13); alternatively, compare with Mann et al. (2009) for a LM perspective that focuses on a forced response.

The Pacific decadal oscillation is a multidecadal pattern of atmospheric and oceanic variability over the North Pacific Ocean. In its warm (cool) or positive (negative) phase, SSTs are above (below) average along the west coast of North America and eastern tropical Pacific and below (above) average in the central North Pacific. Each phase of the PDO lasts from 20 to 30 years, although the short instrumental record precludes establishing a robust spectrum for the PDO. Twentieth-century teleconnection patterns with the PDO show a dipole pattern of wintertime (DJF) North American precipitation, with high precipitation in the southwestern United States and low precipitation in the northwestern United States and across Canada associated with the positive phase of PDO (Mantua et al. 1997) and anomalous dry periods in both northern and southern China (Shen et al. 2006).

The simulated PDO is calculated as the leading order EOF of North Pacific (20°–70°N) monthly SST anomalies, with grid cells having mean ice fraction coverage of 15% or greater removed from the PDO calculation. To eliminate global trends, the area-averaged global SST is subtracted from the monthly SST field. We also remove grid cells with a mean ice fraction of 15% or more from the SST field. The simulated spatial pattern and magnitude of the PDO in the 1850 control simulation compare well with observations, although the tropical–extratropical connections are too weak (Deser et al. 2012). The PDO spectrum shows a modest peak above the 95% confidence level at 4 years in both the control run and the LM, suggesting some influence of ENSO on PDO and peaks around 15 years—similar to the observations. The PDO in both the 1850 control and LM simulations have red power spectra with similar power in the decadal and longer time scales (Fig. 13), suggesting no role for external forcing for modulating the PDO in CCSM4.

The PDO for the LM has been reconstructed using relationships of the PDO with the dominant modes of tree-ring variability or tree-ring sites at PDO-related centers of action for sites in North America and Asia (Biondi et al. 2001; MacDonald and Case 2005; D'Arrigo and Wilson 2006) and an index of droughts and floods in eastern China (Shen et al. 2006). Each of these reconstructions correlate well with the PDO and each other during their calibrations in the twentieth century but do not show any consistent overlap earlier in the LM (Fig. 15). The LM simulation reproduces the amplitude of PDO variability indicated by these reconstructions since 1600 but does not consistently overlap with any of the reconstructions and produces a neutral PDO rather than the strongly negative PDO in the mid-twentieth century. The lack of coherence among the reconstructions and the model suggests that the decadal variations of the PDO may be associated with internal dynamics. The longer MacDonald and Case (2005) PDO reconstruction, which extends backs through the LIA to the MCA, indicates prolonged periods of strongly negative PDO from 993 to 1300 and positive PDO from 1450 to 1550. The LM simulation does not indicate that the MCA compared to the LIA climate states have an influence on the PDO, although the model does simulate centennial periods of negative (1220–1380) and positive (centered on ~1600 and ~1770) PDOs. Further analysis is needed to determine the reasons for these differences. The LM simulation captures the much drier winters in the southwest United States during the MCA than LIA on which the MacDonald and Case reconstruction depends (see discussion in section 4).

b. Atlantic modes: NAO and AMO

The North Atlantic Oscillation is a leading mode of climate variability of the Northern Hemisphere. It is associated with variations in the relative strengths of the normal patterns of lower pressure of the Icelandic low and higher pressures near the Azores and Iberian Peninsula. These pressure oscillations affect the locations and strength of the jet streams and storm tracks over the North Atlantic region, with a strong influence on winter weather in Europe and North America (Thompson and Wallace 1998, 2000; Deser 2000; Thompson et al. 2003). When the NAO is in its positive phase, winters in northern Europe are warmer and wetter and southern Europe and North Africa are cooler and drier. Opposite temperature and precipitation anomalies occur over these regions with the negative phase of the NAO. The instrumental record points to the NAO being an inherent atmospheric pattern of variability that is not primarily forced by coupled atmosphere–land–ocean dynamics (Thompson et al. 2003; Czaja et al. 2003).

We define the NAO as the leading-order EOF of the wintertime (December–March) sea level pressure over the North Atlantic (20°–80°N, 90°W–40°E). This season corresponds to the strongest season for the NAO (Thompson and Wallace 2000; Hurrell and Deser 2009). The simulated magnitude of the NAO index (Fig. 14) and spatial patterns of sea level pressure (SLP), temperature (Fig. 16) and the precipitation impacts to the adjacent continents of Europe and North America

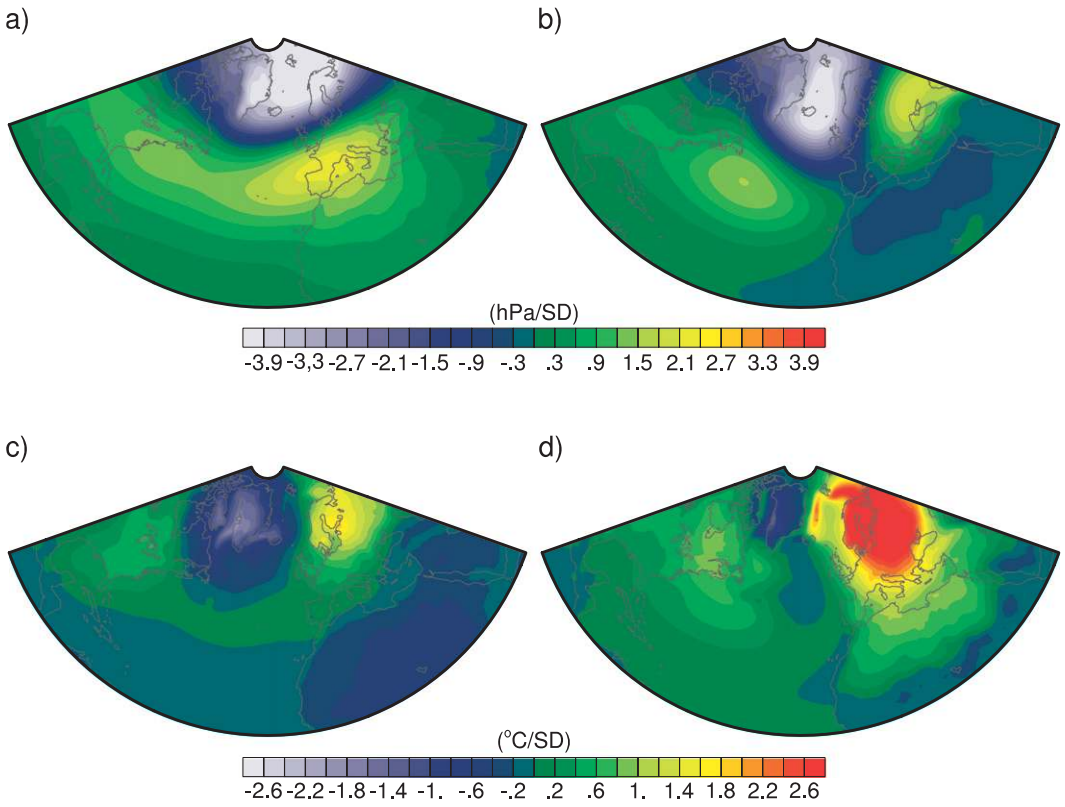

FIG. 16. Regressions of sea level pressure (SLP) on the (a) NAO and (b) AMO, and surface temperature on the (c) NAO and (d) AMO in the CCSM4 LM simulation. The SLP and temperature are plotted in units of hPa and °C per standard deviation of the respective time series (e.g., NAO or AMO).

(Fig. 17) in the LM simulation compare well with observations (Hurrell and Deser 2009; Thompson and Wallace 2000). The NAO has white power spectra in both the LM and control runs with spectral peaks around 3–4, 6, and 8 years (Fig. 13).

Regressions and other relationships between NAO and weather and climate-related variables have been used in proxy-data contexts, including tree rings, speleothems, ice core isotopes, snow accumulation, and phenological data, to reconstruct the NAO for the past millennium (Luterbacher et al. 1999; Glueck and Stockton 2001; Cook et al. 2002; Trouet et al. 2009). Although there are some decades of coherence among the various reconstructions, over much of the common period of the last 400–500 years (Fig. 17) the reconstructions differ in their decadal-to-multidecadal variability, consistent with the conclusions of Cook et al. (2002), who found that their multiproxy NAO reconstruction had the best validation on interannual time scales and the weakest at a multidecadal period. This also is consistent with the power spectra of the CCSM4 simulations, which have no significant spectral peaks for periods longer than a decade.

Trouet et al. (2009) reconstructed a LM NAO index from speleothem-based precipitation records in northwest Scotland and tree-ring based drought records from Morocco. They find a clear tendency toward a persistently positive NAO for approximately 350 years during the MCA. Further evidence for this centennial-scale behavior is that it can explain the relatively warm European temperatures during the MCA. The CCSM4 LM simulations do not reproduce this prolonged positive MCA NAO, although the model decadally smoothed NAO suggests a tendency for the NAO to remain in a positive phase from 1130 to 1330 during the MCA and shorter multidecadal negative phases during the LIA. Several possible reasons could be responsible for the mismatch of the model with the Trouet et al. (2009) reconstruction. These include possible nonstationarity of the precipitation teleconnections to western Europe and northern Africa, although the CCSM4 simulation does not indicate this (Fig. 17, top). Luterbacher et al. (1999) found that the dominant frequencies in their reconstructed NAO varied with season, with significant multidecadal to centennial power during northern spring and summer. The Moroccan February-to-June PDSI

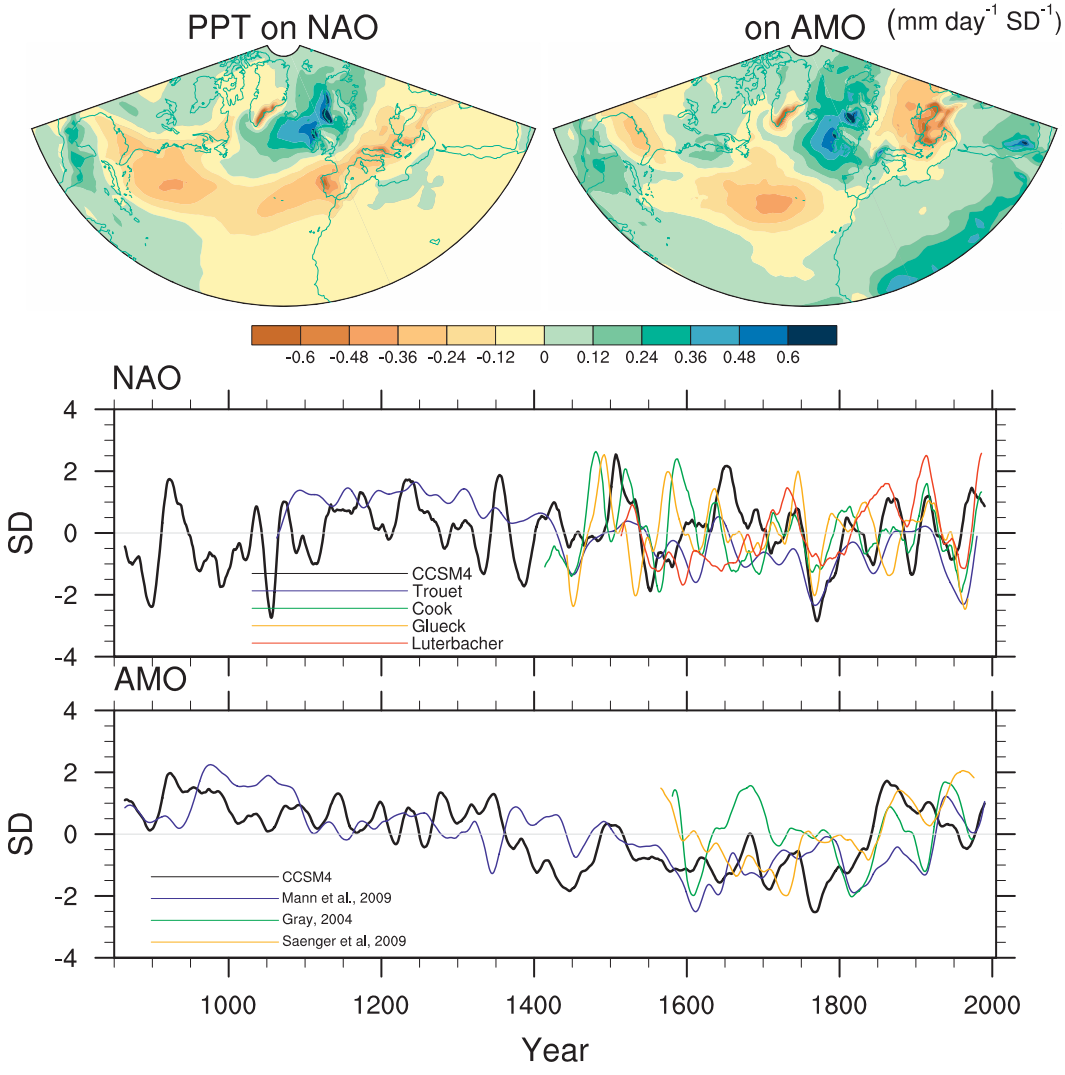

FIG. 17. (top) Regression of total precipitation on the NAO and AMO in the CCSM4 LM simulation, and time series of Last Millennium (middle) NAO and (bottom) AMO from CCSM and proxy-based reconstructions. Model time series are first smoothed with a 30-yr Gaussian smoothing and then are standardized over the entire time (z score over 850–2005, or over the entire length of the individual time series for those proxy-based reconstructions that span a shorter time period).

reconstruction is the basis for the southern node of the NAO dipole in the Trouet et al. reconstruction. We also find that NAO is not always the dominant mode of European climate, with the AMO possibly contributing to the precipitation anomalies during the MCA (as discussed below).

The Atlantic multidecadal oscillation is a quasi-periodic, multidecadal (~60–80 years) variation of basinwide SSTs in the North Atlantic (Schlesinger and Ramankutty 1994; Delworth and Mann 2000), although the observational record of only the last 150 years is too short to adequately characterize the periodicity of the AMO. Model simulations with no change in external forcings find a positive correlation of the AMO with the Atlantic meridional overturning current (AMOC), suggesting that strengthening of the ocean conveyor circulation warms the North Atlantic (Delworth and Mann 2000; Knight et al. 2006). On the other hand, millennial simulations forced with volcanic eruptions and solar variability indicate that oscillations in the AMO lead those in the AMOC (Otterå et al. 2010). Positive (warm) AMO teleconnections are more pronounced during northern summer and the transitional seasons and include warmer and drier conditions over the United States and wetter conditions over the British Isles and western Europe (Sutton and Hodson 2005; Feng et al. 2011; Nigam et al. 2011).

The LM AMO is calculated from the area-weighted North Atlantic (0°–70°N, 90°W–40°E) SST. We remove global trends and influence of sea ice on the SST field by first subtracting the global mean SST (at each time step) and not including any grid cells that have mean ice fraction coverage of 15% or greater before calculating the AMO. The simulated magnitude of the low-passed filtered AMO index (Fig. 17) compares well with observations (Sutton and Hodson 2005). The AMO in both the 1850 control run and the LM simulation have red power spectra with highest power in the decadal and longer time scales (Fig. 13). The AMO has somewhat higher variance in the LM simulation (0.137°C^2) than in the control (0.117°C^2). The spectral peaks near 40 and 80 years in the LM simulation compared with one peak at ~50 years in the 1850 control run suggest that external forcing may be modulating the AMO in CCSM4.

Reconstructions of the LM AMO are available for comparison to the CCSM4 LM simulation, based on North American and European tree rings (Gray et al. 2004), coral growth rates in the Bahamas (Saenger et al. 2009), and the global reconstruction of Mann et al. (2009; based on multiple proxies) (Fig. 17). The lack of strong coherency among the different reconstructions illustrates the difficulty in reconstructing the AMO from regions that can vary in their spatial teleconnections and can be influenced by other factors than the AMO. The LM simulation, as well as the Mann et al. reconstruction, shows a tendency for a positive AMO during the MCA. Although the AMO precipitation teleconnections to Europe and Africa are weaker than those for the NAO, the similar patterns coupled with the positive phase of the AMO during the MCA in the LM simulation suggest that some portion of the proxy responses in the Trouet et al. NAO (derived from proxy records of precipitation) may be influenced by the AMO.

7. Summary and outstanding issues

We have completed a CCSM4 Last Millennium simulation at the standard 1° resolution, the same resolution as the majority of the CCSM4 CMIP5 long-term simulations for the historical and future projection scenarios. This simulation starts at 850 and continues to 1850, where it matches with and is extended as an additional ensemble member of the CCSM4 twentieth-century simulations that end in December 2005. The forcings and boundary conditions for the LM simulation follow the protocols of PMIP3. We include the low solar forcing reconstruction of TSI of VSK, the ice core–based reconstruction of volcanic forcing of Gao et al. (2008), orbital forcings, and the evolution of land use and concentrations of the principal long-lived greenhouse gases.

The Last Millennium simulation with CCSM4 reproduces many but not all of the large-scale climate patterns suggested by historical and proxy-based records. To summarize the results:

1) The LM simulation shows a hockey stick–like pattern in both the Northern and Southern Hemispheres, with cooling to the early 1800s of ~0.5°C for the NH and ~0.3°C for the SH followed by warming to present. Simulated late-twentieth-century hemispheric surface temperatures are much warmer than the surface temperatures simulated during the MCA. Overall the relative warmth exhibited by proxy temperature reconstructions during the MCA (centered around 1000) is somewhat damped in the NH in the LM simulation, particularly in terms of temporal extent into the eleventh and twelfth centuries.
2) Strong global cooling is associated with the large volcanic eruptions, with indications of multidecadal colder climate in response to larger eruptions. The model simulates cooling of ~1.0°–1.5°C after the large eruptions of the late thirteenth, mid-fifteenth, late eighteenth, and early nineteenth centuries, 2–3 times larger than the NH summer anomalies estimated from tree-ring or multiproxy reconstructions, and twentieth-century simulations indicate that the CCSM4 hemispheric response to volcanic eruptions is stronger than observed (Meehl et al. 2012).
3) CCSM4 captures some of the reconstructed patterns of temperature changes over Europe and North America to large volcanic eruptions, although the timings of the composite responses and regional details can be dissimilar. Patterns of simulated precipitation change for the Asian monsoon to large volcanic eruptions have nearly opposite anomalies from those reconstructed from tree-ring chronologies, which was also the case for LM simulations with an earlier version of CCSM.
4) The patterns of simulated surface temperature change and sea ice from the MCA to LIA convey the polar amplification of the responses. This polar amplification of the forced response is also a feature of CSM 1.4 LM simulations and is suggested by the reconstructed differences of Mann et al. (2009), although generally the reconstructions do not extend into the very high latitudes. CCSM4 shows greater sensitivity to solar forcing than CSM 1.4, with comparable amplitudes of warming as the CSM 1.4 medium solar forcing experiment, a forcing that is ~2.5 times the solar forcing used in the CCSM4 LM simulation.
5) The LM simulation does not reproduce La Niña–like cooling in the eastern Pacific at the MCA relative to

the LIA, as has been suggested by proxy reconstructions. It does simulate statistically significant reduced winter $P-E$ over the southwestern United States and reduced summer $P-E$ over the central United States in agreement with proxy records interpreted as indicators of cool and warm half-year precipitation, respectively. The simulated reduced MCA summer soil moisture available for plant growth over most of the United States is also roughly consistent with the NADA PDSI reconstructions. Elsewhere, the simulated $P-E$ anomalies are not statistically different from zero. It is possible that CCSM4 is underestimating the amplitude of these anomalies.

6) The AMO has higher variance and increased power at low frequencies in the LM simulation compared with the 1850 nontransient control run, suggesting long-term oceanic response to natural forcings of the last millennium. The NAO, SAM, PDO, and ENSO show little or no change in their variances, teleconnection patterns, and spectra between the LM simulation and the control run.
7) We do not find a persistent positive NAO or a prolonged period of negative PDO during the MCA suggested by the proxy reconstructions (MacDonald and Case 2005; Trouet et al. 2009), although CCSM4 does simulate centennial periods of negative and positive NAO and PDO. Because both reconstructions use precipitation-correlated proxies calibrated to the twentieth-century instrumental relationship between the index and precipitation, a possible reason for the mismatch may be that other factors have influence (e.g., the AMO for precipitation anomalies over Europe).

Many aspects of the CCSM4 LM simulation remain to be investigated and compared to the proxy reconstructions. Global reconstructions for the MCA show anomalous patterns of temperature, the hydrological cycle, and atmospheric circulation, although a clear single mechanism for explaining these patterns is not yet available (cf. Graham et al. 2011). Detailed temporal and regional reconstructions for the last two millennia or shorter intervals are also available for select regions. Attribution to the externally forced signals for the reconstructed patterns versus internal variability of the climate system should be further investigated. For this purpose, single forcing simulations as well as simulations using differently scaled solar variability and volcanic reconstructions, either for the full 850–2005 period or shorter subintervals, would improve attribution (Goosse et al. 2005; Jungclaus et al. 2010).

The NAO, PDO, and ENSO modes of variability show little or no change in their variances, teleconnection patterns, and spectra between the Last Millennium simulation and the 1850 nontransient control run, yet proxy reconstructions suggest possibly more power at lower frequencies. It is critical to understand if models are underestimating multidecadal to centennial variability of these modes because of the implications for decadal predictions and future projections with these models. Several of the modes derive their reconstructed index values in a way that includes a region of weak teleconnection or use a record that needs to be interpreted in terms of climate. Further model-based work that either uses pseudoproxy generation or incorporates direct simulation of the isotopes used as paleoclimate proxies would help in the latter regard.

The dynamics and thermodynamics of the spatial patterns, amplitude, and timing of response in the simulation to large volcanic eruptions needs to be better understood. Importantly, is the large cooling associated with these eruptions realistic? Timmreck et al. (2010) demonstrate that the cooling effect of the very large 1258 eruption was more consistent with temperature reconstructions when larger aerosol particles are assumed. The transport and size distribution of volcanic aerosols in CCSM4 is parameterized and does not include predictive stratospheric transports. Also, Shindell et al. (2003) determined that interactions with stratospheric ozone can modulate the climatic responses to solar and volcanic forcings. It has also been proposed that the ice core records of a tropical eruption at ~1258 may alternatively be recording multiple eruptions that occurred at high latitudes in both hemispheres (Schneider et al. 2009).

The CCSM4 LM simulation is part of a large suite of simulations completed for CMIP5, including two other paleoclimate simulations for the mid-Holocene and Last Glacial Maximum (Brady et al. 2013), a long 1850 control and ensemble of twentieth-century simulations (Gent et al. 2011), and an ensemble of RCP 2.6, 4.5, 6.0, and 8.5 future projections (Meehl et al. 2012). All of these model data will be archived on the CMIP5 database and available for analysis by the community.

Acknowledgments. We thank A. Mai for running the simulations and G. Strand for processing much of the model output analyzed here. Additionally, we thank the community of scientists and software engineers who have been instrumental in the development of CCSM4. Laura Landrum was supported by the National Science Foundation's Office of Polar Programs, Grant 0908675. The CCSM project is supported by the National Science Foundation and the Office of Science (Biological and Environmental Research program) of the U.S. Department of Energy. Computing resources were provided by the Climate Simulation Laboratory at NCAR's Computational

and Information Systems Laboratory (CISL) sponsored by the National Science Foundation and other agencies.

REFERENCES

Adams, J. B., M. E. Mann, and C. Ammann, 2003: Proxy evidence for an El Niño-like response to volcanic forcing. *Nature,* **426,** 274–278.

Ammann, C. M., and E. R. Wahl, 2007: The importance of the geophysical context in statistical evaluations of climate reconstruction procedures. *Climatic Change,* **85,** 71–88, doi:10.1007/s10584-007-9276-x.

——, G. A. Meehl, W. M. Washington, and C. Zender, 2003: A monthly and latitudinally varying volcanic forcing dataset in simulations of 20th century climate. *Geophys. Res. Lett.,* **30,** 1657, doi:10.1029/2003GL016875.

——, F. Joos, D. S. Schimel, B. L. Otto-Bliesner, and R. A. Tomas, 2007: Solar influence on climate during the past millennium: Results from transient simulations with the NCAR Climate System Model. *Proc. Natl. Acad. Sci. USA,* **104,** 3713–3718.

Anchukaitis, K. J., B. M. Buckley, E. R. Cook, B. I. Cook, R. D. D'Arrigo, and C. M. Ammann, 2010: Influence of volcanic eruptions on the climate of the Asian monsoon region. *Geophys. Res. Lett.,* **37,** L22703, doi:10.1029/2010gl044843.

Bard, E., G. Raisbeck, F. Yiou, and J. Jouzel, 2000: Solar irradiance during the last 1200 years based on cosmogenic nuclides. *Tellus,* **52,** 985–992, doi:10.1034/j.1600-0889.2000.d01-7.x.

Biondi, F., A. Gershunov, and D. R. Cayan, 2001: North Pacific decadal climate variability since 1661. *J. Climate,* **14,** 5–10.

Bitz, C. M., K. M. Shell, P. R. Gent, D. Bailey, G. Danabasoglu, K. C. Armour, M. M. Holland, and J. T. Kiehl, 2012: Climate sensitivity in the Community Climate System Model version 4. *J. Climate,* **25,** 3053–3070.

Booth, R. K., and S. T. Jackson, 2003: A high-resolution record of late-Holocene moisture variability from a Michigan raised bog, USA. *Holocene,* **13,** 863–876.

Bradley, R. S., M. K. Hughes, and H. F. Diaz, 2003: Climate in medieval time. *Science,* **302,** 404–405.

Brady, E. C., B. L. Otto-Bliesner, and N. Rosenbloom, 2013: Sensitivity to glacial forcing in the CCSM4. *J. Climate,* in press.

Braganza, K., J. L. Gergis, S. B. Power, J. S. Risbey, and A. M. Fowler, 2009: A multiproxy index of the El Niño–Southern Oscillation, AD 1525–1982. *J. Geophys. Res.,* **114,** D05106, doi:10.1029/2008jd010896.

Briffa, K. R., 2000: Annual climate variability in the Holocene: Interpreting the message of ancient trees. *Quat. Sci. Rev.,* **19,** 87–105.

——, P. D. Jones, F. H. Schweingruber, and T. J. Osborn, 1998: Influence of volcanic eruptions on Northern Hemisphere summer temperature over the past 600 years. *Nature,* **393,** 450–455.

Brunelle, A., and C. Whitlock, 2003: Holocene vegetation, fire, and climate history from the Selway Mountains, Idaho. *Quat. Res.,* **60,** 307–318.

Büntgen, U., and W. Tegel, 2011: European tree-ring data and the Medieval Climate Anomaly. *PAGES Newsletter,* No. 19, PAGES International Project Office, Bern, Switzerland, 14–20.

Burgman, R., R. Seager, A. Clement, and C. Herweijer, 2010: Role of tropical Pacific SSTs in global medieval hydroclimate: A modeling study. *Geophys. Res. Lett.,* **37,** L06705, doi:10.1029/2009GL042239.

Byrne, R. B. L., S. S. Ingram, and F. Malamud-Roam, 2001: Carbon-isotope, diatom, and pollen evidence for Late Holocene salinity change in a brackish marsh in the San Francisco estuary. *Quat. Res.,* **55,** 66–76.

Christiansen, B., and F. C. Ljundqvist, 2011: Reconstruction of the extratropical NH mean temperature over the last millennium with a method that preserves low-frequency variability. *J. Climate,* **24,** 6013–6034.

Cobb, K. M., C. D. Charles, H. Cheng, and R. L. Edwards, 2003: El Niño/Southern Oscillation and tropical Pacific climate during the last millennium. *Nature,* **424,** 271–276.

Cole, J., and E. Cook, 1998: The changing relationship between ENSO variability and moisture balance in the continental United States. *Geophys. Res. Lett.,* **25,** 4529–4532.

Conroy, J. L., J. T. Overpeck, J. E. Cole, and M. Steinitz-Kannan, 2009: Variable oceanic influences on western North American drought over the last 1200 years. *Geophys. Res. Lett.,* **36,** L17703, doi:10.1029/2009GL039558.

Cook, E. R., cited 2008: North American Summer PDSI Reconstructions, version 2a. NOAA/NGDC Paleoclimatology Program. [Information about the data is available online at ftp://ftp.ncdc.noaa.gov/pub/data/paleo/drought/NAmericanDroughtAtlas.v2/readme-NADAv2-2008.txt; the actual data can be found at http://www.ncdc.noaa.gov/paleo/pdsi08_ts.html.]

——, R. D. D'Arrigo, and M. E. Mann, 2002: A well-verified, multiproxy reconstruction of the winter North Atlantic Oscillation index since AD 1400. *J. Climate,* **15,** 1754–1764.

——, J. Esper, and R. D'Arrigo, 2004a: Extra-tropical Northern Hemisphere land temperature variability over the past 1000 years. *Quat. Sci. Rev.,* **23,** 2063–2074.

——, C. A. Woodhouse, C. M. Eakin, D. M. Meko, and D. W. Stahle, 2004b: Long-term aridity changes in the western United States. *Science,* **306,** 1015–1018.

——, K. J. Anchukaitis, B. M. Buckley, R. D. D'Arrigo, G. C. Jacoby, and W. E. Wright, 2010: Asian monsoon failure and megadrought during the last millennium. *Science,* **328,** 486–489, doi:10.1126/science.1185188.

Crowley, T. J., 2000: Causes of climate change over the past 1000 years. *Science,* **289,** 270–277.

——, S. K. Baum, K. Y. Kim, G. C. Hegerl, and W. T. Hyde, 2003: Modeling ocean heat content changes during the last millennium. *Geophys. Res. Lett.,* **30,** 1932, doi:10.1029/2003GL017801.

——, G. Zielinski, B. Vinther, R. Udisti, K. Kreutzs, J. Cole-Dai, and E. Castellano, 2008: Volcanism and the Little Ice Age. *PAGES Newsletter,* No. 16, PAGES International Project Office, Bern, Switzerland, 22–23.

Czaja, A., A. Robertson, and T. Huck, 2003: The role of coupled processes in producing NAO variability. *North Atlantic Oscillation: Climatic Significance and Environmental Impact, Geophys. Monogr.,* Vol. 134, Amer. Geophys. Union, 147–172.

Danabasoglu, G., S. Bates, B. P. Briegleb, S. R. Jayne, M. Jochum, W. G. Large, S. Peacock, and S. G. Yeager, 2012: The CCSM4 ocean component. *J. Climate,* **25,** 1361–1389.

D'Arrigo, R., and R. Wilson, 2006: On the Asian expression of the PDO. *Int. J. Climatol.,* **26,** 1607–1617, doi:10.1002/joc.1326.

——, ——, and G. Jacoby, 2006: On the long-term context for late twentieth century warming. *J. Geophys. Res.,* **111,** D03103, doi:10.1029/2005JD006352.

——, ——, and A. Tudhope, 2009: The impact of volcanic forcing on tropical temperatures during the past four centuries. *Nat. Geosci.,* **2,** 51–56, doi:10.1038/ngeo393.

Davis, O. K., 2002: Late Neogene environmental history of the northern Bonneville basin: A review of palynological studies. *Great Basin Aquatic Systems History,* R. Hersler, D. B. Madsen, and D. R. Currey, Eds., Smithsonian Contributions

to the Earth Sciences, Vol. 33, Smithsonian Institution Press, 295–307.

Delworth, T. L., and M. E. Mann, 2000: Observed and simulated multidecadal variability in the Northern Hemisphere. *Climate Dyn.,* **16,** 661–676.

Deser, C., 2000: On the teleconnectivity of the ''Arctic Oscillation.'' *Geophys. Res. Lett.,* **27,** 779–782, doi:10.1029/1999GL010945.

——, and Coauthors, 2012: ENSO and Pacific decadal variability in the Community Climate System Model version4. *J. Climate,* **25,** 2622–2651.

Dunbar, R. B., G. M. Wellington, M. W. Colgan, and P. W. Glynn, 1994: Eastern Pacific sea-surface temperature since 1600 A.D.: The $\delta^{18}O$ record of climate variability in Galápagos corals. *Paleoceanography,* **9,** 291–315.

Emile-Geay, J., R. Seager, M. A. Cane, E. C. Cook, and G. H. Haug, 2008: Volcanoes and ENSO over the past millennium. *J. Climate,* **21,** 3134–3148.

——, K. Cobb, M. Mann, and A. T. Wittenberg, 2013: Estimating central equatorial Pacific SST variability over the past millennium. Part II: Reconstructions and uncertainties. *J. Climate,* in press.

Enfield, D. B., A. M. Mestas-Nuñez, and P. J. Trimble, 2001: The Atlantic multidecadal oscillation and its relation to rainfall and river flows in the continental U.S. *Geophys. Res. Lett.,* **28,** 2077–2080.

Esper, J., E. R. Cook, and F. H. Schweingruber, 2002: Low-frequency signals in long tree-ring chronologies for reconstructing past temperature variability. *Science,* **295,** 2250–2253.

Felis, T., A. Suzuki, H. Kuhnert, N. Rimbu, and H. Kawahata, 2010: Pacific decadal oscillation documented in a coral record of North Pacific winter temperature since 1873. *Geophys. Res. Lett.,* **37,** L14605, doi:10.1029/2010GL043572.

Feng, S., O. Hu, and R. J. Oglesby, 2011: Influence of Atlantic sea surface temperatures on persistent drought in North America. *Climate Dyn.,* **37,** 569–586, doi:10.1007/s00382-010-0835-x.

Fischer, E. M., J. Luterbacher, E. Zorita, S. F. B. Tett, C. Casty, and H. Wanner, 2007: European climate response to tropical volcanic eruptions over the last half millennium. *Geophys. Res. Lett.,* **34,** L05707, doi:10.1029/2006GL027992.

Gao, C., A. Robock, and C. Ammann, 2008: Volcanic forcing of climate over the last 1500 years: An improved ice core–based index for climate models. *J. Geophys. Res.,* **113,** D23111, doi:10.1029/2008JD010239.

Gent, P. R., and Coauthors, 2011: The Community Climate System Model version 4. *J. Climate,* **24,** 4973–4991.

Glueck, M. F., and C. W. Stockton, 2001: Reconstruction of the North Atlantic Oscillation, 1429–1983. *Int. J. Climatol.,* **21,** 1453–1465.

Goosse, H., H. Renssen, A. Timmermann, and R. S. Bradley, 2005: Internal and forced climate variability during the last millennium: A model-data comparison using ensemble simulations. *Quat. Sci. Rev.,* **24,** 1345–1360.

Graham, N. E., and Coauthors, 2007: Tropical Pacific–mid-latitude teleconnections in medieval times. *Climatic Change,* **83,** 241–285.

——, C. M. Ammann, D. Fleitmann, K. M. Cobb, J. Luterbacher, 2011: Support for global climate reorganization during the ''Medieval Climate Anomaly.''*Climate Dyn.,* **37,** 1217–1245.

Gray, S. T., L. J. Graumlich, J. L. Betancourt, and G. T. Pederson, 2004: A tree-ring based reconstruction of the Atlantic multidecadal oscillation since 1567 AD. *Geophys. Res. Lett.,* **31,** L12205, doi:10.1029/2004gl019932.

Haug, G. H., K. A. Hughen, D. M. Sigman, L. C. Peterson, and U. Rohl, 2001: Southward migration of the intertropical convergence zone through the Holocene. *Science,* **293,** 1304–1308.

Holland, M. M., and C. M. Bitz, 2003: Polar amplification of climate change in coupled models. *Climate Dyn.,* **21,** 221–232, doi:10.1007/s00382-003-0332-6.

——, D. A. Bailey, B. P. Briegleb, B. Light, and E. Hunke, 2012: Improved sea ice shortwave radiation physics in CCSM4: The impact of melt ponds and aerosols on Arctic sea ice. *J. Climate,* **25,** 1413–1430.

Huang, S., 2004: Merging information from different resources for new insights into climate change in the past and future. *Geophys. Res. Lett.,* **31,** L13205, doi:10.1029/2004GL019781.

Hunke, E. C., and W. H. Lipscomb, 2008: CICE: The Los Alamos sea ice model user's manual, version 4. Los Alamos National Laboratory Tech. Rep. LA-CC-06-012, 76 pp.

Hurrell, J. W., and C. Deser, 2009: North Atlantic climate variability: The role of the North Atlantic Oscillation. *J. Mar. Sys.,* **78,** 28–41, doi:10.1016/j.jmarsys.2008.11.026.

Hurtt, G. C., and Coauthors, 2009: Harmonization of global land-use scenarios for the period 1500-2100 for IPCC-AR5. *iLeaps Newsletter,* No. 7, iLEAPS International Project Office, Helsinki, Finland, 6–8.

Jahn, A., and Coauthors, 2012: Late twentieth-century simulation of Arctic sea ice and ocean properties in the CCSM4. *J. Climate,* **25,** 1431–1452.

Jansen, E., and Coauthors, 2007: Paleoclimate. *Climate Change 2007: The Physical Science Basis,* S. Solomon et al., Eds., Cambridge University Press, 433–497.

Jones, P. D., K. R. Briffa, T. P. Barnett, and S. F. B. Tett, 1998: High-resolution palaeoclimatic records for the last millennium: Interpretation, integration and comparison with general circulation model control-run temperatures. *Holocene,* **8,** 455–471.

——, and Coauthors, 2009: High-resolution palaeoclimatology of the last millennium: A review of current status and future prospects. *Holocene,* **19,** 3–49.

Jungclaus, J. H., and Coauthors, 2010: Climate and carbon-cycle variability over the last millennium. *Climate Past,* **6,** 723–737.

Kaufman, D. S., and Coauthors, 2009: Recent warming reverses long-term Arctic cooling. *Science,* **325,** 1236–1239.

Knight, J. R., C. K. Folland, and A. A. Scaife, 2006: Climate impacts of the Atlantic multidecadal oscillation. *Geophys. Res. Lett.,* **33,** L17706, doi:10.1029/2006gl026242.

Kushnir, Y., R. Seager, M. Ting, N. Naik, and J. Nakamura, 2010: Mechanisms of tropical Atlantic SST influence on North American precipitation variability. *J. Climate,* **23,** 5610–5628.

Lachniet, M. S., S. J. Burns, D. R. Piperno, Y. Asmerom, V. J. Polyak, C. M. Moy, and K. Christenson, 2004: A 1500-year El Niño/Southern Oscillation and rainfall history for the Isthmus of Panama from speleothem calcite. *J. Geophys. Res.,* **109,** D20117, doi:10.1029/2004JD004694.

Laird, K. R., S. C. Fritz, E. C. Grimm, and P. G. Mueller, 1996: Century-scale paleoclimatic reconstructions from Moon Lake, a closed-basin lake in the northern Great Plains. *Limnol. Oceanogr.,* **41,** 890–902.

Lamarque, J.-F., and Coauthors, 2010: Historical (1850–2000) gridded anthropogenic and biomass burning emissions of reactive gases and aerosols: Methodology and application. *Atmos. Chem. Phys.,* **10,** 7017–7039, doi:10.5194/acp-10-7017-2010.

Landrum, L., M. M. Holland, D. Schneider, and E. Hunke, 2012: Antarctic sea ice climatology, variability, and late twentieth-century change in CCSM4. *J. Climate,* **25,** 4817–4838.

Lawrence, D. M., P. E. Thornton, K. W. Oleson, and G. B. Bonan, 2007: The partitioning of evapotranspiration into transpiration,

soil evaporation, and canopy evaporation in a GCM: Impacts on land–atmosphere interaction. *J. Hydrometeor.,* **8,** 862–880.

——, K. W. Oleson, M. G. Flanner, C. G. Fletcher, P. J. Lawrence, S. Levis, S. C. Swenson, and G. B. Bonan, 2011: The CCSM4 land simulation, 1850–2005: Assessment of surface climate and new capabilities. *J. Climate,* **25,** 2240–2260.

Lean, J., cited 2009: Calculations of solar irradiance. [Available online at http://sparcsolaris.geomar.de/input_data.php.]

Li, J., S.-P. Xie, E. R. Cook, G. Huang, R. D'Arrigo, F. Liu, J. Ma, and X.-T. Zheng, 2011: Interdecadal modulation of El Niño amplitude during the past millennium. *Nat. Climate Change,* **1,** 114–118, doi:10.1038/NCLIMATE1086.

Luterbacher, J., C. Schmutz, D. Gyalistras, E. Xoplaki, and H. Wanner, 1999: Reconstruction of monthly NAO and EU indices back to AD 1675. *Geophys. Res. Lett.,* **26,** 2745–2748.

MacDonald, G. M., and R. A. Case, 2005: Variations in the Pacific decadal oscillation over the past millennium. *Geophys. Res. Lett.,* **32,** L08703, doi:10.1029/2005GL022478.

Mann, M. E., and P. D. Jones, 2003: Global surface temperatures over the past two millennia. *Geophys. Res. Lett.,* **30,** 1820, doi:10.1029/2003GL017814.

——, R. S. Bradley, and M. K. Hughes, 1998: Global-scale temperature patterns and climate forcing over the past six centuries. *Nature,* **392,** 779–787.

——, M. A. Cane, S. E. Zebiak, and A. Clement, 2005: Volcanic and solar forcing of the tropical Pacific over the past 1000 years. *J. Climate,* **18,** 447–456.

——, Z. Zhang, M. K. Hughes, R. S. Bradley, S. K. Miller, S. Rutherford, and F. Ni, 2008: Proxy-based reconstructions of hemispheric and global surface temperature variations over the past two millennia. *Proc. Natl. Acad. Sci. USA,* **105,** 13 252–13 257, doi:10.1073/pnas.0805721105.

——, and Coauthors, 2009: Global signatures and dynamical origins of the Little Ice Age and Medieval Climate Anomaly. *Science,* **326,** 1256–1260.

——, J. D. Fuentes, and S. Rutherford, 2012: Underestimation of volcanic cooling in tree-ring-based reconstructions of hemispheric temperatures. *Nat. Geosci.,* **5,** 202–205, doi:10.1038/NGEO1394.

Mantua, N. J., S. R. Hare, Y. Zhang, J. M. Wallace, and R. C. Francis, 1997: A Pacific interdecadal climate oscillation with impacts on salmon production. *Bull. Amer. Meteor. Soc.,* **78,** 1069–1079.

McCabe, G., M. A. Palecki, and J. L. Betancourt, 2004: Pacific and Atlantic Ocean influences on multidecadal drought frequency in the United States. *Proc. Natl. Acad. Sci. USA,* **101,** 4136–4141, doi:10.1073/pnas.0306738101.

McGovern, T. H., 1991: Climate, correlation, and causation in Norse Greenland. *Arctic Anthropol.,* **28,** 77–100.

McGregor, S., and A. Timmermann, 2011: The effect of explosive tropical volcanism on ENSO. *J. Climate,* **24,** 2178–2191.

——, ——, and O. Timm, 2010: A unified proxy for ENSO and PDO variability since 1650. *Climate Past,* **6,** 1–17.

Meehl, G. A., and Coauthors, 2012: Climate system response to external forcings and climate change projections in CCSM4. *J. Climate,* **25,** 3661–3683.

Millspaugh, S. H., C. Whitlock, and P. J. Bartlein, 2000: Variations in fire frequency and climate over the past 17 000 yr in central Yellowstone National Park. *Geology,* **28,** 211–214.

Moberg, A., D. M. Sonechkin, K. Holmgren, N. M. Datsenko, and W. Karlén, 2005: Highly variable Northern Hemisphere temperatures reconstructed from low- and high-resolution proxy data. *Nature,* **433,** 613–617.

Mohr, J. A., C. Whitlock, and C. N. Skinner, 2000: Postglacial vegetation and fire history, eastern Klamath Mountains, California, USA. *Holocene,* **10,** 587–601.

Neale, R. B., J. H. Richter, and M. Jochum, 2008: The impact of convection of ENSO: From a delayed oscillator to a series of events. *J. Climate,* **21,** 5904–5924.

——, J. Richter, S. Park, P. H. Lauritzen, S. J. Vavrus, P. J. Rasch, and M. Zhang, 2013: The mean climate of the Community Atmosphere Model (CAM4) in forced SST and fully coupled experiments. *J. Climate,* in press.

Neukom, R., and Coauthors, 2011: Multiproxy summer and winter surface air temperature field reconstructions for southern South America covering the past centuries. *Climate Dyn.,* **37,** 35–51, doi:10.1007/s00382-010-0793-3.

Nigam, S., B. Guan, and A. Ruiz-Barradas, 2011: Key role of the Atlantic multidecadal oscillation in 20th century drought and wet periods over the Great Plains. *Geophys. Res. Lett.,* **38,** L16713, doi:10.1029/2011GL048650.

Oerlemans, J., 2005: Extracting a climate signal from 169 glacier records. *Science,* **308,** 675–677.

Oglesby, R., S. Feng, Q. Hu, and C. Rowe, 2011: The role of the Atlantic multidecadal oscillation on medieval drought in North America: Synthesizing results from proxy data and climate models. *Global Planet. Change,* **84-85,** 56–65, doi:10.1016/j.gloplacha.2011.07.005.

Oman, L., A. Robock, G. Stenchikov, G. A. Schmidt, and R. Ruedy, 2005: Climatic response to high-latitude volcanic eruptions. *J. Geophys. Res.,* **110,** D13103, doi:10.1029/2004jd005487.

Otterå, O. H., M. Bentsen, H. Drange, and L. L. Suo, 2010: External forcing as a metronome for Atlantic multidecadal variability. *Nat. Geosci.,* **3,** 688–694.

Pollack, H. N., and J. E. Smerdon, 2004: Borehole climate reconstructions: Spatial structure and hemispheric averages. *J. Geophys. Res.,* **109,** D11106, doi:10.1029/2003jd004163.

Pongratz, J., C. H. Reick, T. Raddatz, and M. Claussen, 2008: A reconstruction of global agricultural areas and land cover for the last millennium. *Global Biogeochem. Cycles,* **22,** GB3018, doi:10.1029/2007GB003153.

Quinn, W. H., V. T. Neal, and S. E. Antunez de Mayolo, 1987: El Niño occurrences over the past four and half centuries. *J. Geophys. Res.,* **92C,** 14 449–14 461.

Rajagopalan, B., E. Cook, U. Lall, and B. K. Ray, 2000: Spatiotemporal variability of ENSO and SST teleconnections to summer drought over the United States during the twentieth century. *J. Climate,* **13,** 4244–4255.

Richter, J. H., and P. J. Rasch, 2008: Effects of convective momentum transport on the atmospheric circulation in the Community Atmosphere Model, version 3 (CAM3). *J. Climate,* **21,** 1487–1499.

Rutherford, S., M. E. Mann, T. J. Osborn, R. S. Bradley, K. R. Briffa, M. K. Hughes, and P. D. Jones, 2005: Proxy-based Northern Hemisphere surface temperature reconstructions: Sensitivity to methodology, predictor network, target season, and target domain. *J. Climate,* **18,** 2308–2329.

Saenger, C., A. L. Cohen, D. W. Oppo, R. B. Halley, and J. E. Carilli, 2009: Surface-temperature trends and variability in the low-latitude North Atlantic since 1552. *Nat. Geosci.,* **2,** 492–495.

Schlesinger, M. E., and N. Ramankutty, 1994: An oscillation in the global climate system of period 65–70 years. *Nature,* **367,** 723–726.

Schmidt, G. A., and Coauthors, 2012: Climate forcing reconstructions for use in PMIP simulations of the Last Millennium (v1.1). *Geosci. Model Dev.,* **5,** 1850191, doi:10.5194/gmd-5-185-2012.

Schneider, D. P., C. M. Ammann, B. L. Otto-Bliesner, and D. S. Kaufman, 2009: Climate response to large, high-latitude and low-latitude volcanic eruptions in the Community Climate System Model. *J. Geophys. Res.,* **114,** D15101, doi:10.1029/2008jd011222.

Schubert, S. D., M. J. Suarez, P. J. Pegion, R. D. Koster, and J. T. Bacmeister, 2004: On the cause of the 1930s Dust Bowl. *Science,* **303,** 1855–1859.

——, and Coauthors, 2009: A U.S. CLIVAR project to assess and compare the responses of global climate models to drought-related SST forcing patterns: Overview and results. *J. Climate,* **22,** 5251–5272.

Seager, R., N. Graham, C. Herweijer, A. L. Gordon, Y. Kushnir, and E. Cook, 2007a: Blueprints for medieval hydroclimate. *Quat. Sci. Rev.,* **26,** 2322–2336, doi:10.1016/j.quascirev.2007.04.020.

——, and Coauthors, 2007b: Model projections of an imminent transition to a more arid climate in southwestern North America. *Science,* **316,** 1181–1184, doi:10.1126/science.1139601.

Servonnat, J., P. Yiou, M. Khodri, D. Swingedouw, and S. Denvil, 2010: Influence of solar variability, CO_2 and orbital forcing between 1000 and 1850 AD in the IPSLCM4 model. *Climate Past,* **6,** 445–460.

Shen, C. M., W.-C. Wang, W. Gong, and Z. Hao, 2006: A Pacific decadal oscillation record since 1470 AD reconstructed from proxy data of summer rainfall over eastern China. *Geophys. Res. Lett.,* **33,** L03702, doi:10.1029/2005gl024804.

Shindell, D. T., G. A. Schmidt, R. L. Miller, and M. E. Mann, 2003: Volcanic and solar forcing of climate change during the pre-industrial era. *J. Climate,* **16,** 4094–4107.

Smith, R. D., and Coauthors, 2010: The Parallel Ocean Program (POP) reference manual. Los Alamos National Laboratory Tech. Rep. LAUR-10-01853, 141 pp.

Solomon, S., D. Qin, M. Manning, M. Marquis, K. Averyt, M. M. B. Tignor, H. L. Miller Jr., and Z. Chen, Eds., 2007: *Climate Change 2007: The Physical Science Basis.* Cambridge University Press, 996 pp.

Stahle, D. W., and Coauthors, 1998: Experimental dendroclimatic reconstruction of the Southern Oscillation. *Bull. Amer. Meteor. Soc.,* **79,** 2137–2152.

Sutton, R. T., and D. L. R. Hodson, 2005: Atlantic Ocean forcing of North American and European summer climate. *Science,* **309,** 115–118.

Thompson, D. W. J., and J. M. Wallace, 1998: The Arctic oscillation signature in the wintertime geopotential height and temperature fields. *Geophys. Res. Lett.,* **25,** 1297–1300.

——, and ——, 2000: Annular modes in the extratropical circulation. Part I: Month-to-month variability. *J. Climate,* **13,** 1000–1016.

——, S. Lee, and M. P. Baldwin, 2003: Atmospheric processes governing the Northern Hemisphere annular mode/North Atlantic Oscillation. *The North Atlantic Oscillation: Climatic Significance and Environmental Impact, Geophys. Monogr.,* Vol. 134, Amer. Geophys. Union, 81–112.

Timmreck, C., and Coauthors, 2010: Limited temperature response to the very large AD 1258 volcanic eruption. *Geophys. Res. Lett.,* **37,** L21708, doi:10.1029/2009GL040083.

Trenberth, K. E., and A. Dai, 2007: Effects of Mount Pinatubo volcanic eruption on the hydrological cycle as an analog of geoengineering. *Geophys. Res. Lett.,* **34,** L15702, doi:10.1029/2007gl030524.

Trouet, V., J. Esper, N. E. Graham, A. Baker, J. D. Scourse, and D. C. Frank, 2009: Persistent positive North Atlantic oscillation mode dominated the medieval climate anomaly. *Science,* **324,** 78–80, doi:10.1126/science.1166349.

Verleyen, E., and Coauthors, 2011: Post-glacial regional climate variability along the East Antarctic coastal margin—Evidence from shallow marine and coastal terrestrial records. *Earth Sci. Rev.,* **104,** 199–212.

Vieira, L. E. A., S. K. Solanki, N. A. Krivova, and I. Usoskin, 2011: Evolution of the solar irradiance during the Holocene. *Astron. Astrophys.,* **531,** A6, doi:10.1051/0004-6361/201015843.

Wahl, E. R., and C. M. Ammann, 2007: Robustness of the Mann, Bradley, Hughes reconstruction of Northern Hemisphere surface temperatures: Examination of criticisms based on the nature and processing of proxy climate evidence. *Climatic Change,* **85,** 33–69, doi:10.1007/s10584-006-9105-7.

——, and ——, 2010: Examining the forced response of past regional climate to guide selection of general circulation models for regional analyses. *Extended Abstracts, 22nd Conf. on Climate Variability and Change,* Atlanta, GA, Amer. Meteor. Soc., 7.2. [Available online at https://ams.confex.com/ams/90annual/techprogram/paper_159714.htm.]

——, and C. Morrill, 2010: Toward understanding and predicting monsoon patterns. *Science,* **328,** 437–438, doi:10.1126/science.1188926.

——, and J. Smerdon, 2012: Comparative performance of paleoclimate field and index reconstructions derived from climate proxies and noise-only predictors. *Geophys. Res. Lett.,* **39,** L06703, doi:10.1029/2012GL051086.

——, H. R. Diaz, and C. Ohlwein, 2011: A pollen-based reconstruction of summer temperature in central North America and implications for circulation patterns during medieval times. *Global Planet. Change,* **84-85,** 66–74, doi:10.1016/j.gloplacha.2011.10.005.

Wigand, P. E., 1997: A late Holocene pollen record from Lower Pahranagat Lake, southern Nevada, USA: High-resolution paleoclimatic records and analysis of environmental responses to climate change. *Proc. 13th Annual Pacific Climate (PACLIM) Workshop,* California Department of Water Resources Tech. Rep. 53, 63–77.

——, and D. Rhode, 2002: Great Basin vegetation history and aquatic systems: The last 150,000 years. *Great Basin Aquatic Systems History,* R. Hershler, D. B. Madsen, and D. R. Currey, Eds., Smithsonian Contributions to Earth Sciences Series, Vol. 33, Smithsonian Institution Press, 309–367.

Wilson, R., E. Cook, R. D'Arrigo, N. Riedwyl, M. N. Evans, A. Tudhope, and R. Allan, 2010: Reconstructing ENSO: The influence of method, proxy data, climate forcing and teleconnections. *J. Quat. Sci.,* **25,** 62–78.

Zhao, J., R. P. Turco, and O. B. Toon, 1995: A model simulation of Pinatubo volcanic aerosols in the stratosphere. *J. Geophys. Res.,* **100,** 7315–7328.

Zhong, Y., G. H. Miller, B. L. Otto-Bliesner, M. M. Holland, D. A. Bailey, D. P. Schneider, and A. Geirsdottir, 2011: Centennial-scale climate change from decadally-paced explosive volcanism: A coupled sea ice-ocean mechanism. *Climate Dyn.,* **37,** 2373–2387, doi:10.1007/s00382-010-0967-z.